Factors controlling CO_2 exchange on timescales from hourly to decadal at Harvard Forest

S. Urbanski,[1] C. Barford,[2] S. Wofsy,[3] C. Kucharik,[2] E. Pyle,[3] J. Budney,[3] K. McKain,[3] D. Fitzjarrald,[4] M. Czikowsky,[4] and J. W. Munger[3]

Received 21 August 2006; revised 25 October 2006; accepted 17 January 2007; published 9 May 2007.

[1] We analyzed 13 years (1992–2004) of CO_2 flux data, biometry, and meteorology from a mixed deciduous forest in central Massachusetts. Annual net uptake of CO_2 ranged from 1.0 to 4.7 Mg-C $ha^{-1}yr^{-1}$, with an average of 2.5 Mg-C $ha^{-1}yr^{-1}$. Uptake rates increased systematically, nearly doubling over the period despite forest age of 75–110 years; there were parallel increases in midsummer photosynthetic capacity at high light level (21.5–31.5 μmole $m^{-2}s^{-1}$), woody biomass (101–115 Mg-C ha^{-1} from 1993–2005, mostly due to growth of one species, red oak), and peak leaf area index (4.5–5.5 from 1998–2005). The long-term trends were interrupted in 1998 by sharp declines in photosynthetic capacity, net ecosystem exchange (NEE) of CO_2, and other parameters, with recovery over the next 3 years. The observations were compared to empirical functions giving the mean responses to temperature and light, and to a terrestrial ecosystem model (IBIS2). Variations in gross ecosystem exchange of CO_2 (GEE) and NEE on hourly to monthly timescales were represented well as prompt responses to the environment, but interannual variations and long-term trends were not. IBIS2 simulated mean annual NEE, but greatly overpredicted the amplitude of the seasonal cycle and did not predict the decadal trend. The drivers of interannual and decadal changes in NEE are long-term increases in tree biomass, successional change in forest composition, and disturbance events, processes not well represented in current models.

Citation: Urbanski, S., C. Barford, S. Wofsy, C. Kucharik, E. Pyle, J. Budney, K. McKain, D. Fitzjarrald, M. Czikowsky, and J. W. Munger (2007), Factors controlling CO_2 exchange on timescales from hourly to decadal at Harvard Forest, *J. Geophys. Res.*, *112*, G02020, doi:10.1029/2006JG000293.

1. Introduction

[2] Terrestrial ecosystems mediate a large portion of the CO_2 flux between the Earth's surface and the atmosphere, with approximately 120 Pg CO_2-C yr^{-1} taken up by gross photosynthesis and roughly the same amount respired back to the atmosphere [*Prentice et al.*, 2001]. Imbalances between photosynthesis and respiration create CO_2 sinks and sources, which in aggregate have accounted for uptake of 1–2 Pg-C yr^{-1} by terrestrial ecosystems between 1980 and 2000 [*Battle et al.*, 2000; *Ciais et al.*, 1995; *Hicke et al.*, 2002; *Keeling et al.*, 1996; *McGuire et al.*, 2001; *Myneni et al.*, 2001; *Tans et al.*, 1990]. The magnitudes of sinks and sources have fluctuated on annual and longer timescales owing to variable climate, land use change, disturbance by fire and pests, and changes in the age distribution and species composition of the ecosystem [*Battle et al.*, 2000; *Barford et al.*, 2001; *Dunn et al.*, 2007; *Houghton*, 2000].

[3] The relationships between controlling variables and the net terrestrial CO_2 flux are not quantitatively understood at the process level. Proposed mechanisms for recent net uptake include legacies of prior land use and disturbance, longer growing seasons, fertilization by rising CO_2, and deposition of industrial fixed nitrogen [*Goodale et al.*, 2002; *Houghton*, 2002; *Schimel et al.*, 2000, 2001]. The factors must be quantitatively understood in order to predict how carbon storage will change with time [*Schimel et al.*, 2001; *Wofsy and Harriss*, 2002].

[4] Net ecosystem exchange of CO_2 (NEE) is the sum of canopy photosynthesis (gross ecosystem exchange, GEE) and ecosystem respiration (R), separate processes with different physical and biological controls that are linked over long timescales at the ecosystem level. In practice these may be distinguished by equating GEE to the light-dependent part of NEE, and setting R = NEE − GEE. (Note that by convention, uptake of CO_2 from the atmosphere has negative sign, so GEE <0 and R > 0.)

[5] Ecosystem respiration includes contributions from autotrophs (vegetation) and heterotrophs (free living and symbiotic microorganisms and fauna in the soil) [*Bowden*

[1]Fire Sciences Laboratory, Rocky Mountain Research Station, USDA Forest Service, Missoula, Montana, USA.
[2]Center for Sustainability and the Global Environment (SAGE), Nelson Institute for Environmental Studies, University of Wisconsin-Madison, Madison, Wisconsin, USA.
[3]Division of Engineering and Applied Sciences and Department of Earth and Planetary Sciences, Harvard University, Cambridge, Massachusetts, USA.
[4]Atmospheric Sciences Research Center, State University of New York at Albany, Albany, New York, USA.

0148-0227/07/2006JG000293

et al., 1993; *Ryan and Law*, 2005; *Trumbore*, 2006]. Field studies of R have identified temperature, soil moisture, nutrient availability, stocks of living and dead biomass, ecosystem productivity, and seasonal carbon allocation as controlling factors [*Boone et al.*, 1998; *Davidson et al.*, 2006; *Hogberg et al.*, 2001; *Ryan and Law*, 2005; *Savage and Davidson*, 2001; *Whitehead et al.*, 2004]. GEE is controlled by canopy development and nutrient status, light, temperature, ambient humidity, CO_2 concentration, and soil moisture [*Field and Mooney*, 1986; *Larcher*, 1995; *Ruimy et al.*, 1996]. Mechanistic terrestrial ecosystem models typically use subsets of these factors to drive functions that predict carbon fluxes. R is usually simulated as an exponential function of temperature modified by soil moisture [*Davidson et al.*, 2006]. GEE is usually specified as a function of ambient CO_2, intercepted flux of photosynthetically active radiation (PAR), foliar N, soil moisture, and in many cases, vapor pressure deficit and temperature, with parameters based on a combination of ecosystem-scale and leaf-level measurements [e.g., *McGuire et al.*, 2001; *Adams et al.*, 2004].

[6] Assessments of ecosystem carbon balance under changing climate, based on these models, are very uncertain [*Davidson and Janssens*, 2006]. Several studies predict that increased ecosystem respiration could exceed productivity gains under rising CO_2 and temperature, creating a net-positive feedback to the climate system [*Cao and Woodward*, 1998; *Doney et al.*, 2006; *Friedlingstein et al.*, 2006; *Kirschbaum*, 1995]. However, predictions of climate-driven changes in R are highly dependent on the assumed functional dependence on temperature [*Joos et al.*, 2001; *Jones et al.*, 2003] and soil moisture [*Fung et al.*, 2005]. Recent work questions the control of R by temperature [*Giardina and Ryan*, 2000; *Hogberg et al.*, 2001], the timescales of the temperature response [*Braswell et al.*, 1997; *Kirschbaum*, 2004; *Knorr et al.*, 2005; *Reichstein et al.*, 2005], and the assumed effects of soil moisture [*Doney et al.*, 2006].

[7] Long-term eddy flux data are powerful new integral constraints on the carbon balance of whole ecosystems that provide key data to help to elucidate underlying controlling factors [*Law et al.*, 2002; *Sanderman et al.*, 2003]. Given the significant interannual variability of midlatitude ecosystem carbon exchange, decadal length carbon flux data are necessary to identify secular trends in carbon exchange associated with the gradual influence of ecosystem dynamics, environment (e.g., CO_2 fertilization, nitrogen deposition) and climate change. These data are critical to testing and improving ecosystem models, since, like the models, they span timescales from hours to decades and represent the whole ecosystem.

[8] We report here a 13-year study of NEE in a New England mixed deciduous forest (Harvard Forest), measured using the eddy-covariance technique, intended to help understand the current regime of carbon sequestration in forest ecosystems, and to gain insight into the factors that will control carbon balance in the future. Harvard Forest is the longest-running eddy flux site in the world. The long-term NEE, and validation against biometric data, have been reported previously [*Barford et al.*, 2001; *Goulden et al.*, 1996a, 1996b; *Wofsy et al.*, 1993]. Now the data record (1992–2004) is long enough to identify emerging long-term trends and to quantify the important effects and lingering legacies of disturbance. Hence the goals of this paper are (1) to quantify the instantaneous (hourly) ecosystem carbon exchange response to controlling climate variables (temperature and sunlight), averaged over a decade; (2) to separate responses to climate and weather variations from underlying changes in ecosystem processes and structure; (3) to quantify long-term trends in carbon exchange and ecosystem function; and (4) to assess the mechanisms responsible for seasonal, interannual and long-term deviations of ecosystem carbon exchange from decadal means.

[9] We developed a suite of empirical, ecophysiologically-based models (denoted "Model-0", and variants) to quantify the mean functional responses of carbon exchange to weather (sunlight, temperature, soil moisture) and season. Mean ecosystem responses were obtained as a model fit to the decade-long, internally consistent data set of NEE, temperature, light, and canopy development (79,000 hours of data at Harvard Forest); these were subtracted from hourly, daily, seasonally and annually aggregated data to identify deviations from mean behavior. We discuss both short-term deviations and long-term trends in NEE, R, and GEE with respect to key environmental and ecological factors (e.g., biomass dynamics, disturbance, nutrient status), and we identify the drivers of long-term net carbon exchange.

[10] Dynamic ecosystem models attempt to simulate allocation and storage of organic matter. We assess how well these models capture the long-term patterns at Harvard Forest, by comparing results from the Integrated BIosphere Simulator - 2 (IBIS-2), to Model-0, which does not simulate pools of organic matter. IBIS-2 is a global ecosystem model based on dynamic biosphere–climate system interactions [*Foley et al.*, 1996; *Kucharik et al.*, 2000, 2006], driven here by Harvard Forest weather.

1.1. Site Description

[11] NEE, fluxes of latent and sensible heat, and associated meteorological variables have been measured since 1989 at the Harvard Forest Environmental Monitoring Site (HFEMS), located on the Prospect Hill tract of Harvard Forest (42.538N, 72.171W, elevation 340 m) [*Goulden et al.*, 1996a; *Wofsy et al.*, 1993]. The area surrounding the tower is dominated by red oak (*Quercus rubra*) and red maple (*Acer rubrum*), with scattered stands of Eastern hemlock (*Tsuga canadensis*), white pine (*Pinus strobus*) and red pine (*P. resinosa*) (see http://www.as.harvard.edu/chemistry/hf/hfsite.html for further details, and http://www.as.harvard.edu/data/nigec-data.html for data access). The forest contained $\sim$100 Mg-C ha^{-1} in live aboveground woody biomass (AGWB) when the HFEMS was established [*Barford et al.*, 2001]. About 1/3 of the existing red oaks were established prior to 1895, another 1/3 prior to 1930, and the rest before 1940 (N. Pederson, Columbia University, private communication, 2003); hence the stand is 75–110 years old. Although the stand was affected by a hurricane blowdown in 1938, many of the canopy trees now present would have already been established in the understory. Nearly continuous forest extends for several km northwest, west and southwest of the tower, the predominant wind directions. A small forested swamp is located NW of the tower; it expanded in 2000 owing to beaver

activity which has since ceased, leaving the flowage blocked. In the summer of 2000, a selective, commercial harvest took place 300 m to the S–SE of the tower, fortunately a direction sampled rarely at the tower. The selective harvest removed 42.8 m^3 ha^{-1} of timber and 22.5 Mg-C ha^{-1} of AGWB on 43 ha.

[12] In 1993, 40 plots for biometric measurements were established in stratified-random positions along eight 500 m transects, running SW and NW from the tower along the dominant wind directions [*Barford et al.*, 2001] (ftp://ftp.as.harvard.edu/pub/nigec/HU_Wofsy/hf_data/ecological_data/). Ongoing ground-based measurements include above ground woody increment, leaf litter flux, leaf area index (LAI), tabulations of tree mortality and recruitment, and surveys of woody debris. Periodic measurements include green foliage and leaf litter chemistry and soil respiration during the growing season, and a recent study [*Liu et al.*, 2006] measured the respiration rates of coarse woody debris.

1.2. Flux Measurements

[13] The eddy-covariance technique is used to measure fluxes of CO_2, momentum, and sensible and latent heat at 30 m at the HFEMS [*Goulden et al.*, 1996b; *Wofsy et al.*, 1993]. The mixing ratio of CO_2 within the canopy is measured at 8 levels (z = 29, 24, 18, 13, 7.5, 4.5, 0.8, 0.3 m). The flux of photosynthetically active radiation (PAR) is measured above (29 m) and below (13 m) the canopy. Vertical profiles of air temperature and relative humidity are measured at 8 levels from 2.5 m to 29 m. Soil temperature is measured using an array of 6 thermistors buried at the base of the litter layer (10 cm) and two additional thermistors at 20 cm and 50 cm. Upwelling and downwelling PAR, total shortwave radiation, and longwave radiation are measured by Atmospheric Sciences Research Center (ASRC) at State University of New York (SUNY) at Albany [*Moore et al.*, 1996]. The ASRC group also measures eddy fluxes of momentum and sensible heat at 30 m and below the canopy (11 m). Radiation measurements obtained by the ASRC group have been essential for filling gaps in the PAR data set, and the existence of 3 sensors for measuring above-canopy downwelling solar radiation has allowed us to ensure the long-term stability of PAR measurements, a critical detail for long-term studies of ecosystem function (see Appendix A).

1.2.1. Time-Integrated Data

[14] To characterize the ecosystem carbon cycle, we must integrate hourly measurements of carbon exchange and driving climate variables to monthly, annual and decadal timescales, requiring estimates of carbon exchange when data are missing owing to power outages, equipment failure or invalid data. Equipment failure and data rejection reduce the average annual data coverage of our NEE measurements to about 50%, a fraction typical of continuous eddy covariance measurement sites [*Falge et al.*, 2001a]. Temporal aggregation of the hourly NEE measurements is performed using rigorously tested time-integration algorithms that estimate missing hourly NEE observations with a robust ensemble estimation approach (Appendix B). Nighttime observations of NEE are used to estimate daytime ecosystem respiration (NEE_{night} = R) proximate in time, enabling the inference of the light-dependent portion of ecosystem exchange of CO_2 (GEE = NEE − R). We carefully estimated the uncertainties and potential biases in annual sums of NEE, R and GEE by comparing three variants of time integration algorithms: non-linear regression, look-up tables, and diel mean cycle (Appendix B) [cf. *Falge et al.*, 2001a, 2001b], the latter being non-parametric. Because gap-filled data are dependent on an assumed model structure, they are generally not suitable for extracting other model parameters. Hence the parameters of Model-0 were obtained using only unfilled data for hourly NEE.

[15] Missing environmental data must also be estimated to analyze carbon exchange, especially hourly PAR and air temperature, and daily precipitation and soil moisture (Appendix B). Most environmental data can be assembled using actual observations from nearby meteorological stations (Appendix A). Continuous soil moisture profiles were measured at the site only between 1997–1999 (K. E. Savage and E. A. Davidson, personal communication, 2000). We used these data to parameterize a simple two-layer soil hydrology model (see Appendix D), providing continuous estimated values constrained by hundreds of observations and driven by meteorology data from the site. Growing season soil moisture for the study was reconstructed with the calibrated soil hydrology model. The entire climate driver data set is available at ftp://ftp.as.harvard.edu/pub/nigec/HU_Wofsy/hf_data/Final/Filled/HF_9204_filled.

1.2.2. Modeling and Analysis

1.2.2.1. Model-0

[16] The empirical model (Model-0) uses the homogeneous, internally consistent Harvard Forest NEE and climate data sets to represent the instantaneous ecosystem response to temperature and sunlight within a given season and phenological period, using equation (1). Parameters a_1 and a_2 define respiration and its short-term temperature response, respectively, and parameters a_3 and a_4 modify the rate of canopy photosynthesis. The driving variables are air temperature at 2.5 m (T), its seasonal mean ($\langle T \rangle_{mean}$), and above-canopy PAR.

$$NEE = a_1 + a_2 * \left(T - \langle T \rangle_{mean}\right) + PRI * \frac{a_3 * PAR}{a_4 + PAR}. \quad (1)$$

Observations of light attenuation that capture the development of the canopy, i.e., the PAR ratio index (PRI), are included as a driving variable in the late spring (Appendix C).

[17] To parameterize Model-0, nine years (1992–2000) of hourly, u* filtered NEE, T, and PAR observations were sorted into 8 phenologically defined seasonal periods, ranging from 25 to 125 days in length (see Appendix C). During the dormant seasons (late fall and winter), there is still some weak uptake of CO_2 due to conifer photosynthesis; in these time intervals ecosystem dependence on PAR was simplified to a linear response (a_3*PAR). A non-linear least squares procedure (tangent-linear) was used to derive the set of optimized Model-0 parameters for each season for a total of 30 parameters, $\{a_{i,m}\}$, where i = 1–3 (equation (1)), and m = 1–8 (season), and $\{a_{4,m}\}$, m = 1–6 (see Appendix C).

1.2.2.2. Model-0 and Soil Moisture

[18] Analysis of the residuals between CO_2 flux data and Model-0 at seasonal scales indicates a dependence of NEE on soil moisture in the mid-summer, but not during other seasons. There was no significant correlation between

ecosystem respiration (nighttime NEE, either observed or Model-0 residuals) and soil moisture in any season, even though small-scale (chamber) studies have identified soil moisture as an important factor influencing soil respiration at Harvard Forest [*Savage and Davidson*, 2001]. Previous analyses of CO_2 fluxes, climate data [*Freedman et al.*, 2001] and leaf level studies [*Cavender-Bares and Bazzaz*, 2000] at Harvard Forest have indicated the importance of drought stress limitations on photosynthesis under certain conditions. Hence we evaluated the role of soil moisture at HFEMS by incorporating this factor into variants of the Model-0 formulation.

[19] Soil water content was measured as ~6 hour averages using TDR probes inserted horizontally into the soil at 4 levels, in both well drained upland and poorly drained wetland soil plots located 150 m NW and 150 m SW of the HFEMS tower, respectively (K. E. Savage and E. A. Davidson, personal communication, 2000). We used the soil moisture profiles for 1997–1999 to parameterize a simple two-layer bucket-type soil hydrology model (Appendix D). The algorithm design is similar to the water balance methodology used to calculate Palmer soil drought indices [*Palmer*, 1965], with the soil profile divided into a shallow "surface layer" and a deep "under layer" (See Figure D1 in Appendix D). Model simulations of surface layer and under layer volumetric soil moisture content spanning the growing season (DOY 100–300) were computed with a 5-day time step. Five-day sums of latent heat flux, measured on top of the HFEMS tower, and precipitation, measured at a meteorological station 1.5 km away, drive the model. Four adjustable parameters define (1 and 2) the water capacity of the soil in each layer, (3) the flux of water between the soil and the atmosphere, and (4) the transport of water from the surface layer into the under layer. Two additional model parameters control water loss from the under layer during periods of strong water depletion. The depth of the bucket model layers were fixed to match the depth of the soil moisture probes in the measurement pits, and the bucket model parameters were optimized to fit the in situ soil moisture observations (K. E. Savage and E. A. Davidson, personal communication, 2000). Independent model parameters were derived for well-drained and poorly drained soils (Table D1 in Appendix D); parameters were optimized using the genetic algorithm [*Carroll*, 1996].

[20] The reconstructed soil moisture time series from the two-layer model (above) were used to drive three modified versions of Model-0 for Harvard Forest (Model-0a, b, c), in order to define the effects of variability in soil moisture and to explore the best model representation of these effects. The Model-0a equation includes a function of soil moisture that may be interpreted as an additional respiration term and was designed to test for a soil moisture role in regulating ecosystem respiration. The Model-0b equation simulates soil moisture stress on photosynthesis by multiplying the GEE term by a soil moisture stress factor (see Appendix D).

[21] The third modified form of Model-0 (Model-0c) uses a hydraulic resistor/capacitor-type algorithm to calculate canopy water potential [*Jones*, 1978], which is then integrated into the basic Model-0 equation. Water retention curves (K. E. Savage and E. A. Davidson, personal communication, 2000) were used to convert the estimated volumetric soil moisture to matric potential (Ψ_S). The daily canopy water potential was assumed to behave periodically and to depend on light, as calculated using equation (2). The canopy matric potential (Ψ_C) was included as an additional term in the original Model-0 equation that modifies gross carbon assimilation (equation (3)). Equations (2) and (3) were solved iteratively to obtain the optimized parameter set $\{a_1, \ldots, a_5; C, D\}$ for each season.

$$\frac{d\Psi_C}{dt} = (\Psi_S - \Psi_C)*C - D*E, \tag{2}$$

where $E = \{1 + a_5 *\Psi_C\} * \frac{a_3 * PAR}{a_4 + PAR}$,

$$NEE = a_1 + a_2[T - \langle T \rangle] + \{1 + a_5 * \Psi_C\} * \frac{a_3 * PAR}{a_4 + PAR}. \tag{3}$$

[22] In the hydraulic resistor/capacitor equation (equation (2)), Ψ_S and Ψ_C are the matric potential of the soil and canopy, respectively; the product DE is the canopy water transpiration rate, and C is the time constant for refilling the canopy with water. Model-0c uses GEE as a proxy for the canopy transpiration flux and parameter D is equivalent to $1/(\alpha c)$, where c is the canopy water capacitance and α is the canopy water use efficiency. The parameter a_5 controls the direction and magnitude of the Ψ_C influence on NEE. Fitted parameters and further description of Model-0a, b, c are presented in Appendix D, with results summarized in Figure 13 in section 2.3.3 and Figure D4 in Appendix D.

1.2.3. IBIS-2

[23] IBIS-2, like most biophysical models of NEE, produces a representation of the mean ecosystem response (e.g., carbon exchange with the atmosphere) to changing environmental conditions above (e.g., cloudiness, precipitation, temperature, wind, humidity), below (e.g., soil water and temperature) and within (e.g., CO_2, temperature, light, water, wind) a vegetative canopy at a specific geographic location. To calculate ecosystem response, IBIS (version 2.6) utilizes several sub-models within a hierarchical conceptual framework [i.e., *Kucharik et al.*, 2000, Figure 1], which is organized with respect to the submodels' characteristic temporal scales.

1.2.3.1. Land Surface Processes

[24] The land surface submodel simulates the energy, water, carbon, and momentum balance of the soil-plant-atmosphere system at a half-hourly time step using the LSX land surface scheme of *Pollard and Thompson* [1995]. IBIS-2 includes two vegetation layers with eight potential forest plant functional types (PFTs) in the upper canopy, and two grass (cool and warm season) and two shrub PFTs in the lower canopy. The model state description includes six soil layers of varying thicknesses to a 4-m depth (0–10, 10–25, 25–50, 50–100, 100–200, 200–400 cm), which are parameterized with biome-specific root biomass distributions of *Jackson et al.* [1996], and varied soil texture and corresponding physical attributes. Physiologically based formulations of leaf-level photosynthesis [*Farquhar et al.*, 1980], stomatal conductance [*Ball*, 1988; *Collatz et al.*, 1991, 1992] and respiration [*Ryan*, 1991] control canopy exchange processes. Leaf-level photosynthesis is scaled to the canopy level by assuming that photosynthesis is pro-

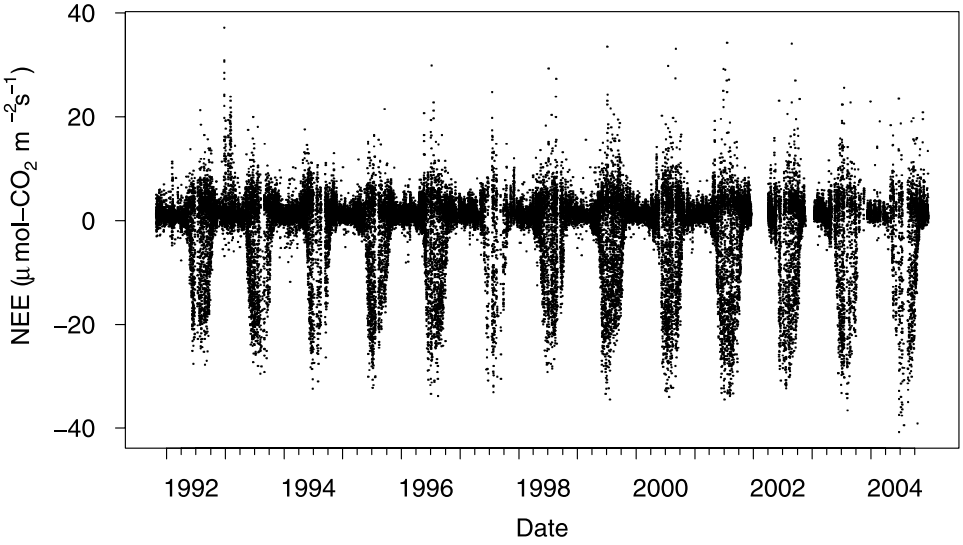

Figure 1. Observed Net Ecosystem Exchange (NEE) at Harvard Forest EMS from 28 October 1991 through 31 December 2004. Only valid observations with u* > 20 cm s^{-1} are shown.

portional to the absorbed photosynthetically active radiation (APAR) within the canopy.

1.2.3.2. Vegetation Dynamics

[25] IBIS-2 can simulate changes in vegetation structure on an annual time step by allowing plants to compete for light and water from common resource pools. The competition between plants is driven by differences in resource availability (light and water), carbon allocation, phenology (evergreen, deciduous), leaf-form (needleleaf, broadleaf), and photosynthetic pathway (C3 versus C4) [*Foley et al.*, 1996; *Kucharik et al.*, 2000]. However, to compare with observations in this study, the forest canopy height, maximum leaf area index (LAI), tree species composition and phenological characteristics (date of budburst and leaf fall) were prescribed using observations from Harvard Forest [*Kucharik et al.*, 2006].

1.2.3.3. Soil Biogeochemistry

[26] IBIS-2 accounts for daily flows of carbon and nitrogen through vegetation, detritus, and soil organic matter similarly to the CENTURY model [*Parton et al.*, 1987] and the biogeochemistry model of *Verberne et al.* [1990]. The current version of the model does not account for leaf nitrogen effects on photosynthesis, or the effects of herbivory, disease, or weather-related disturbance on LAI and accumulated biomass.

[27] IBIS-2 was driven by observed 30-minute meteorological data from Harvard Forest (1992–2004), consisting of air temperature, downward shortwave radiation, wind speed, and relative humidity. Precipitation data were only available at a daily time step; thus, half-hourly data were derived by dividing the daily values by 48. Downward longwave radiation was calculated using *Brutsaert*'s [1975] formulae. For the purposes of parameterizing leaf-level photosynthesis, the maximum rate of carboxylation (V_{cmax}) was set at 55 μmol m^{-2} s^{-1} (at 15°C [*Williams et al.*, 1996]). Dominant soil textural information (sand/silt/clay fractions) was obtained from the STATSGO data set [*Miller and White*, 1998]. The atmospheric CO_2 concentration was set constant at 360 ppm for all simulations.

2. Results

2.1. Eddy-Covariance Observations

[28] From 28 October 1991 to 31 December 2004 there were 51629 valid hourly NEE observations (out of a possible 115,536), with the criterion that CO_2 flux and storage were both measured and friction velocity (u*) exceeded 20 cm s^{-1}. The observations (Figure 1) show the clear seasonal pattern of active photosynthesis and respiration in the summer months and low respiration over the winter. Interannual variations in the magnitude of summer uptake rates, and summer and winter respiration rates, are evident in the data. These observations are integrated to compute sums over daily to annual intervals using multiple filling algorithms (Appendix B). Wherever the filled data are used we take the average of the three approaches. Annual sums using the individual filling algorithms agreed within 0.3 Mg-C ha^{-1} yr^{-1} for all years, except 1998. Estimates of total net carbon uptake (13-year sum) differ by less than 2% (range 31.7 to 32.1 Mg-C ha^{-1}) among the filling procedures.

[29] The forest surrounding HFEMS has been a net CO_2 sink each year throughout the study period (Figure 2 and Table 1). Annual NEE averaged -2.5 Mg-C ha^{-1} yr^{-1}, with a range of −1.0 to −4.7 Mg-C ha^{-1} yr^{-1} (negative values denote uptake from the atmosphere). Figure 2 and Table 1 include estimated uncertainties for the annual sums of NEE derived using a comprehensive bootstrap procedure (see Appendix B).

[30] The variability of annual NEE is dominated by growing season processes (Figure 3); except in 1993, anomalies of annual NEE from the 13-year mean closely track anomalies in growing season NEE ($r^2 = 0.79$, p-value <0.001). For example, extreme CO_2 exchange years 1998 and 2001 were 40% and 190% of the 13-year mean,

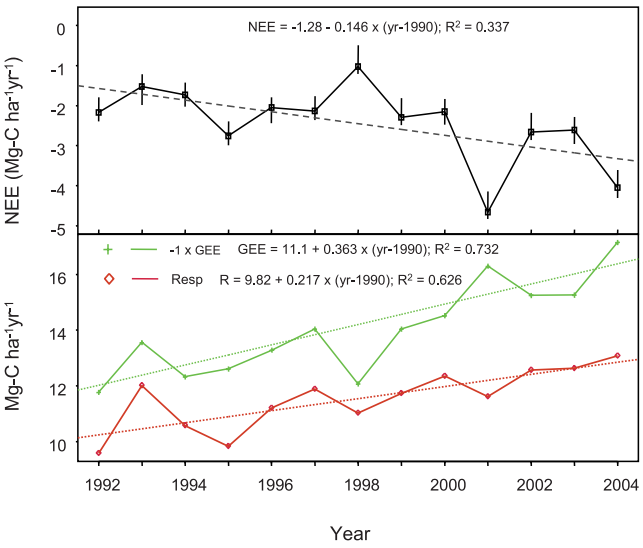

Figure 2. (top) Annual sums of observed NEE at Harvard Forest. Net uptake by the biosphere is negative. (bottom) Annual sums of respiration (R) and gross ecosystem exchange (GEE). R is derived from nighttime NEE and scaled to full day by temperature responses determined over moving windows. GEE is computed as the difference NEE – R and integrated to annual sums. Note that the sign of GEE is inverted (i.e., plotted as production to allow a condensed scale on the y axis). The dashed lines show linear least squares fits. P values for the NEE, GEE, and R trends are 0.0376, 0.0002, and 0.001, respectively. With the 1998 anomaly, excluded p values are 0.0235, 3×10^{-5}, and 0.0018. The NEE error bars in the top plot are the 95% confidence interval estimated using a comprehensive bootstrap procedure (see Appendix B).

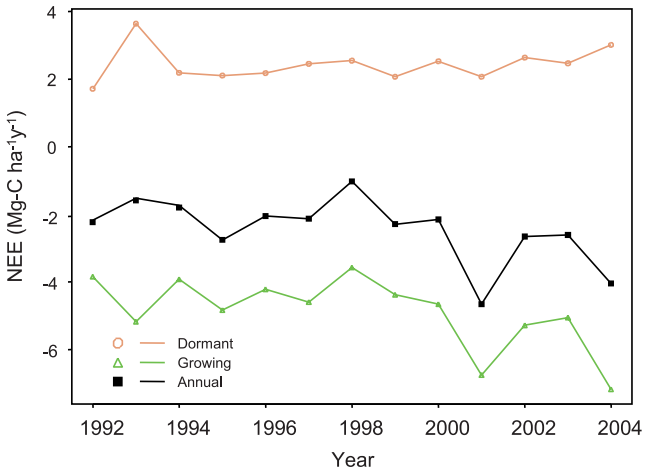

Figure 3. Annual sums of NEE for 1992–2004 (black line with squares) are compared to sums of NEE over the dormant (brown line with circles) and growing season (green line with triangles). Annual sums are calculated for "ecological years," starting on 28 October which corresponds to the ecosystem transition from carbon uptake to release after the leaves have fallen. Dormant season is 28 October to 15 April and growing season is 15 April to 27 October. The annual trends and anomalies are most closely matched by the growing season NEE sums.

respectively; both of these NEE anomalies were driven by anomalies in GEE (Table 1 and Figure 2) and reflect activity predominantly in the growing season (Figure 3). During ecological year 2001, Harvard Forest sequestered 4.7 Mg-C ha^{-1} (Table 1). Although the annual sum of R in 2001 was near average, the magnitude of the annual sum of GEE was one of the largest in the 13-year data set, indicating that enhanced photosynthesis drove the large net uptake of CO_2. Conversely, weak GEE in 1998 resulted in anomalously low net carbon uptake, despite slightly below-average R.

[31] The full 13 years of CO_2 exchange measurements show trends of increasing R and GEE (Figure 2) significant at the 99% confidence level. Ecosystem respiration and GEE have increased by 2–3% yr^{-1} since measurements began, and the increase in GEE has exceeded the increase

Table 1. Annual and Seasonal Sums of NEE, R, and GEE at Harvard Forest From 1992–2004

Ecological Year[a]	Annual[b]				Dormant[b]			Growing[b]		
	NEE	95% CI	R	GEE	NEE	R	GEE	NEE	R	GEE
1992	−2.2	−.225 +.375	9.6	−11.8	1.7	2.1	−0.4	−3.9	7.5	−11.3
1993	−1.5	−.466 +.305	12.0	−13.5	3.7	4.1	−0.4	−5.2	7.9	−13.1
1994	−1.7	−.294 +.304	10.6	−12.3	2.2	2.6	−0.4	−3.9	8.0	−11.9
1995	−2.8	−.237 +.360	9.8	−12.6	2.1	2.6	−0.5	−4.9	7.2	−12.1
1996	−2.0	−.388 +.255	11.2	−13.3	2.2	2.6	−0.4	−4.3	8.6	−12.8
1997	−2.1	−.231 +.372	11.9	−14.0	2.5	2.9	−0.4	−4.6	9.0	−13.6
1998	−1.0	−.186 +.532	11.0	−12.1	2.6	3.1	−0.5	−3.6	8.0	−11.6
1999	−2.3	−.194 +.481	11.7	−14.0	2.1	2.6	−0.5	−4.4	9.1	−13.5
2000	−2.2	−.321 +.319	12.4	−14.5	2.5	3.1	−0.6	−4.7	9.3	−13.9
2001	−4.7	−.176 +.519	11.6	−16.3	2.1	2.4	−0.3	−6.8	9.2	−16.0
2002	−2.7	−.203 +.478	12.6	−15.2	2.6	3.2	−0.6	−5.3	9.4	−14.7
2003	−2.6	−.349 +.323	12.6	−15.3	2.5	2.9	−0.4	−5.1	9.8	−14.8
2004	−4.1	−.260 +.439	12.9	−17.1	3.0	3.6	−0.5	−7.2	9.4	−16.5
Mean	−2.42	±0.03[c]	11.5	−14.0	2.4	2.9	−0.5	−4.9	8.6	−13.5
Standard deviation	1.0	-	1.1	1.6	0.5	0.5	0.1	1.1	0.8	1.6

[a]"Ecological years" are 28 October of preceding year to 27 October of the nominal year; for example, ecological year 1998 runs from 28 October 1997 through 27 October 1998. Dormant season runs from 28 October through 10 April of the following year; growing season is from 11 April to 27 October.
[b]Data are in Mg-C ha^{-1} yr^{-1} or Mg-C ha^{-1} $season^{-1}$.
[c]Here 2× is the range from three different filling algorithms. Calendar year annual sums of NEE, R, and GEE are given Table B1, Appendix B.

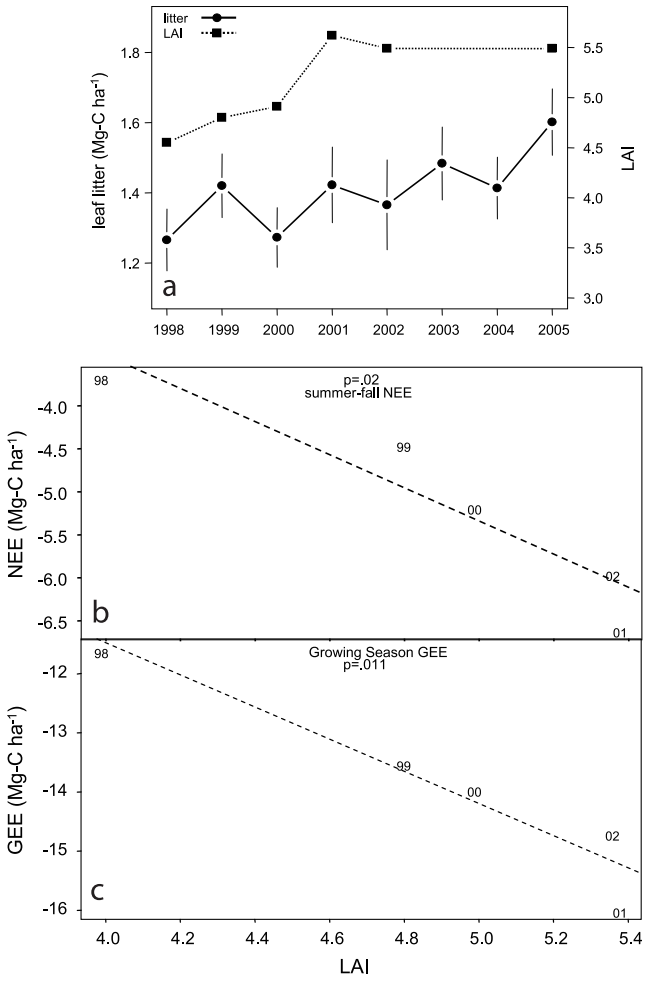

Figure 4. (a) Total annual leaf litter input and mid summer LAI. LAI was measured on dates ranging from late July through late August. LAI values for 2000–2002 were taken from measurements made at a subset of BigFoot plots [*Gower*, 2004], which fell within the same area sampled by the HFEMS biometric plots. A comparison in 2005 of LAI measured at the selected BigFoot plots and HFEMS plots showed no significant difference, although methodological consistency between measurements made at the two plot groups is uncertain. Error bars show 95% confidence intervals for variability among plots. (b) Season NEE versus midsummer LAI. (c) Growing season sums of observed GEE versus midsummer LAI.

in R, leading to a corresponding increase in the magnitude of NEE (0.15 Mg-C $ha^{-1}yr^{-1}$ more uptake), significant at 95% level. As with the anomalies in NEE annual sums, the long-term trends in R and GEE are driven by growing season carbon exchange, as demonstrated by the weak trend in dormant season NEE (i.e., R) (Figure 3).

2.2. Biometric Data

[32] Observations of LAI have been made throughout the growing season for most years since 1998 using the LICOR LAI-2000 system at 30-40 fixed points surrounding HFEMS. From a low of 4.5 m^2 m^{-2} in 1998, LAI increased to about 5.5 m^2 m^{-2} and has been steady since 2001 (Figure 4a; these values include a contribution of ~0.9 m^2 m^{-2} from stems and twigs). Annual litter inputs also increased slightly (Figure 4a and Table 2). Over the period 1998–2002, the residuals between growing season NEE and Model-0, and growing season NEE and GEE, have been significantly correlated with LAI (R^2 = 0.89, 0.87, 0.87, respectively) (Figures 4b–4c). Notably, the GEE at high light levels (photosynthetic capacity) closely tracked the trends in LAI (Figure 15 in section 3.2).

[33] Evidently the recent trends of increasing NEE and GEE have been associated at least in part with thickening of the canopy, prompting questions as to the driver of increased LAI. The observed increase in AGWB (15% over the period), primarily in red oak, is a likely candidate. Over the past decade, annual aboveground woody increment (AGWI) varied between 1 and 2.5 Mg-C $ha^{-1}yr^{-1}$ (not including mortality; see Figure 5a). Peaks in AGWI (2002 and 2005) have lagged the peaks in NEE (2001, 2004) by one year. Annual mortality has been quite variable. In part this variance is an artifact because tree mortality can be protracted and our procedure accounts for mortality through a single survey during the growing season to find trees with no live foliage; dying trees are not counted until all the branches have died. Furthermore tree mortality follows episodic stress events, which also contributes to large variance. AGWB has increased steadily from 101 Mg-C ha^{-1} in 1993 to over 115 Mg-C ha^{-1} in 2005, for an average annual increment of 1.04 Mg-C ha^{-1} (including mortality). This increment should comprise about half of the total biometric carbon budget at the site, as previously shown for 1993–2000 [*Barford et al.*, 2001]; increases in woody roots, coarse woody debris, and soil carbon contributed the other half. Red oak AGWB increased by more than 20% in the 12 years between 1993 and 2005 (Figure 5b), while the total woody biomass of all other species increased by ~7%. The flux of oak leaf litter appears to have increased by ~15% in the 5 years for which we have data, 1998—2003 (Table 2), consistent with this view.

2.3. Model-0 Analysis

[34] The Model-0 parameters $\{a_{i,m}\}$ given in Figure 6 and Table 3 have clear biophysical significance. The mean monthly respiration parameter, $a_{1,}$ increases approximately linearly with monthly mean temperature $<T>_{mean}$, reflecting increased metabolic rates and living biomass in warmer months. Slowing of respiration from early summer to late summer clearly emerges in the parameters $\{a_{1,m}\}$ (Figure 6). *Savage and Davidson* [2001] observed this effect in their chamber data from the Harvard Forest site and attributed it

Table 2. Annual Leaf Litterfall at Harvard Forest From 1998–2004[a]

Year	Total	Oak	Maple	Other *spp*
1998	1.27	0.63	0.34	0.30
1999	1.42	0.67	0.35	0.40
2000	1.27	0.58	0.34	0.36
2001	1.42	0.69	0.34	0.39
2002	1.37	0.71	0.23	0.43
2003	1.48	0.71	0.32	0.45
2004	1.41	NA	NA	NA
2005	1.60	NA	NA	NA

[a]Unit is Mg-C ha^{-1}.

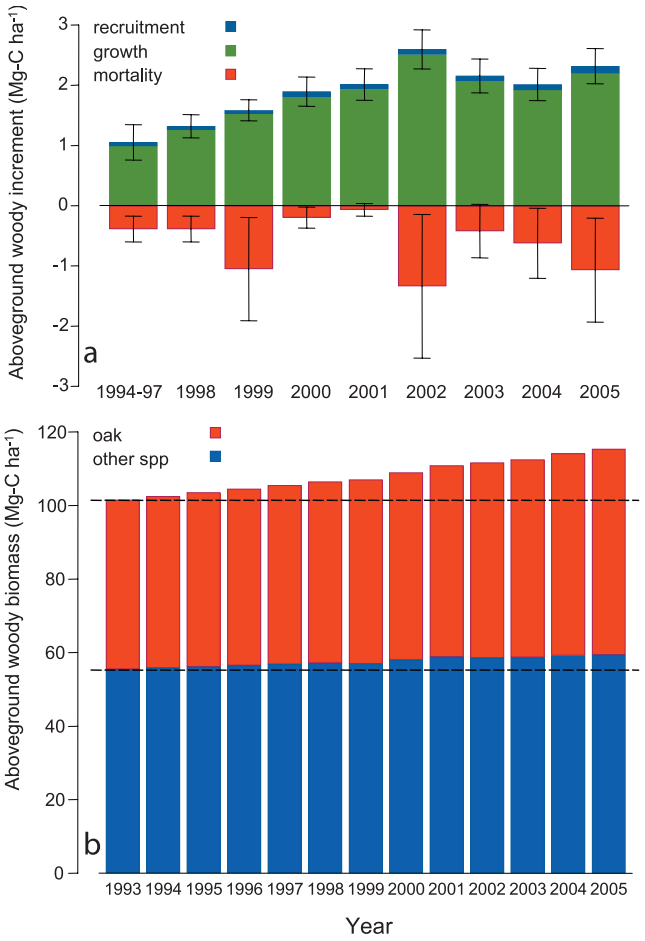

Figure 5. (a) Gross annual fluxes in live above ground woody biomass with 95% confidence limits of mortality and the sum of growth + recruitment. Growth, shown by the green bars, is determined from diameter measurements of all trees ≥10 cm in diameter at breast height (DBH), which are converted to biomass using allometric equations [*Tritton and Hornbeck*, 1982]. Blue bars show the recruitment of new trees into the ≥10 cm DBH size-class. Red bars show losses from the live biomass pool due to mortality, which is determined once per year at the peak of growing season by observation that a tree has no living foliage. Annual fluxes for 1994–1997 are given as a multiyear average because annual biomass surveys were not conducted during that time period. Note that the difference between growth and mortality is not the carbon balance of the site. See *Barford et al.* [2001] for a full accounting of the site carbon balance. (b) Total living aboveground biomass in trees ≥10 cm DBH. Each bar is divided by the contribution from red oaks and all other species. Oaks account for most of biomass increment; red maple is not growing significantly, and other species make a minor contribution to the total biomass. Horizontal lines provide references for assessing growth of oaks versus all other species.

to limited soil moisture; it might also reflect depletion of the labile organic matter from the previous year's litter or reduction in root activity as the growing season nears its end. The ratio $-a_3/a_4$ corresponds to canopy quantum yield at low sun angles; Model-0 obtains values (0.05 to 0.06) consistent with expectations based on maximum quantum yields for C_3 plants (0.06 to 0.07) [*Farquhar et al.*, 1980], allowing for photon reflection and absorption by soil and stems.

2.3.1. Hourly Timescale

[35] The Model-0 fits for hourly data in each month are illustrated in Figure 7 for a typical year. During summer predicted NEE closely matches observations because variations are largely driven by the strong dependence of GEE on light, but in winter, when NEE is dominated by R with a weak dependence on temperature, the fits are poor. This pattern is repeated for all years (Figure 8); R^2 values exceed 0.8 for summer months but approach 0 in winter.

2.3.2. Longer Timescales

[36] Model-0 predictive skill diminishes as longer aggregation intervals are considered. At monthly scales the predicted NEE and GEE still match the observations quite well; R^2 values exceed 0.9 for comparison of predictions and observations. The relationship between monthly predicted and observed R has an R^2 of 0.84, with somewhat more scatter evident. For seasonal intervals, the R^2 for predicted and observed NEE, GEE, and R are 0.97, 0.97, and 0.88, respectively (Figure 9), but the apparently good fit is illusory because it largely captures the annual cycle; deviations of seasonal sums from the mean cycle over 13 years are not well simulated (see Figure 10). Fitting statistics for the phenological seasons are given in Table 4. During the dormant seasons, the predictions have large biases, and slopes of a linear fit versus temperature differ from Table 3. R^2 values are low (or negative, implying that the variance of the residuals (Model-Observed) is larger than for the observations alone for this aggregation interval) in the dormant season and rise to maximum values of 0.65 for early summer season.

[37] Annual sums of NEE, GEE and R are not well captured by Model-0. The model does account for about half of the anomalies in 1998, 2001 and 2004, but observed long-term trends in NEE, GEE and R are not associated with trends in environmental forcing parameters (Figure 11).

[38] The simple PAR and T relationships of Model-0 best describe the hourly to seasonal-scale variability of NEE in the early growing season. This is the period when the ecosystem is most responsive to sunlight and temperature; the canopy is newly developed and daily insolation is at its maximum. The ecosystem is typically well watered and processes related to soil moisture, such as plant water stress, are usually unimportant. However, we observed that wind direction, which affects the contribution from wetlands and coniferous stands, and the phenology index were important variables in spring; these drivers vary on daily and longer timescales.

2.3.3. Soil Moisture Influence

[39] During most intervals, Model-0 residuals had no significant relationship to soil moisture for either seasonal or monthly intervals. However, summertime NEE residuals were affected, being more positive (i.e., weaker uptake) at low soil moisture, and August NEE showed a significant dependence on soil moisture ($R^2 = 0.48$, $p < 0.05$). Figure 12 shows the relationships of ecosystem respiration (nighttime NEE), daytime NEE, as well as Model-0 residuals with estimated soil moisture for the midsummer season. Nighttime NEE (respiration) had no significant correlation to soil

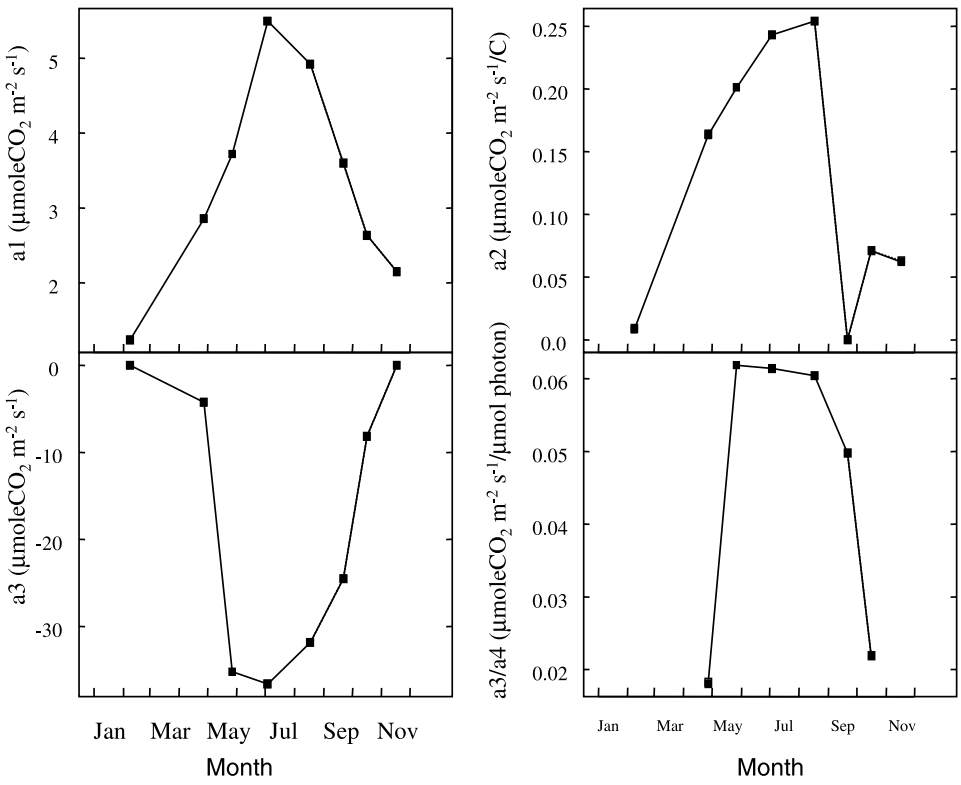

Figure 6. Model-0 parameter values plotted against time of year for the eight seasonal periods (see Appendix C).

moisture, in mid-summer or at any other time, contrary to expectations. The correlation between observed daytime NEE and soil moisture was significant ($p < .1$, $r^2 = 0.32$, $t = -1.55$), as was the relationship with Model-0 residuals ($p < .05$, $R^2 = 0.45$, $t = -2.42$).

[40] The simple model of canopy matric potential (equations (2) and (3)) improved model accuracy for NEE in midsummer by reducing modeled CO_2 uptake under dry soil conditions, and even captured much of the diel cycle of NEE (see Figure D4 in Appendix D). The output of Model-0 with canopy matric potential is a significant improvement over the basic Model-0 for mid-summer, yielding a 40% reduction in RMSE (see Table D2 in Appendix D), and capturing ~70% of interannual variability in this season (Figure 13 and Table D2 in Appendix D). Most of the improvement is seen in dry years (1995, 1998, 1999) in which systematic afternoon depression of GEE was most significant (see Figure D4 in Appendix D).

2.4. IBIS-2 Analysis

[41] To test whether a mechanistic ecosystem model could capture observed patterns in NEE, we simulated the HFEMS data using IBIS-2, driven by observed meteorology and initialized with site characteristics (section 1.2.3). Figures 11 and 14 show annual and monthly sums, respectively. IBIS-2 simulations reproduced the 13-year annual mean NEE at HFEMS (observed = -2.5 Mg-C ha^{-1} yr^{-1} versus IBIS-2 = -2.3 Mg-C ha^{-1} yr^{-1}), but failed to capture the interannual variability of NEE (Figure 11, top). Moreover, seasonal variations were not well simulated,

Table 3. Optimized Model-0 Parameters and Fitting Statistics[a]

Season	Range	N	a1	a2	a3	a4	<T>mean	RMSE	MAE	r^2
Late fall	301–340	4114	2.15	0.06	0.00	NA	3.4	1.61	1.17	0.10
Winter	341–100	13,654	1.24	0.01	0.00	NA	−2.5	1.86	1.03	0.00
Early spring	101–130	3403	2.85	0.16	−4.28	237	9.0	1.72	1.22	0.39
Late spring[b]	131–160	3286	3.70	0.20	−35.19	571	13.9	3.02	2.15	0.79
Early summer	161–205	4250	5.49	0.24	−36.62	597	19.0	4.5	3.28	0.83
Midsummer	206–250	3765	4.88	0.25	−31.77	525	19.1	4.54	3.18	0.80
Late summer	251–275	2649	3.63	−0.01	−24.39	489	14.5	3.51	2.51	0.79
Early fall	276–300	2790	2.62	0.07	−8.15	376	9.2	2.66	1.89	0.43

[a]Model-0 is calibrated using hourly observations of u* - filtered NEE, PAR, and T for DOY 301, 1991, through DOY 300, 2000. Season is Model-0 season, range is DOY range for Model-0 season (see Appendix C), and N is number of valid observations used in calibration. Units are as follows: a_1, μmole CO_2 m^{-2} s^{-1}; a_2, μmole CO_2 m^{-2} s^{-1} $°C^{-1}$; a_3, μmole CO_2 m^{-2} s^{-1}; a_4, μmole-photons m^{-2} s^{-1}; and $<T>_{mean}$, °C. RMSE, root mean square error; MAE, mean absolute error; r^2, coefficient of determination.

[b]Late spring data were obtained using PRI (see text and Appendix C).

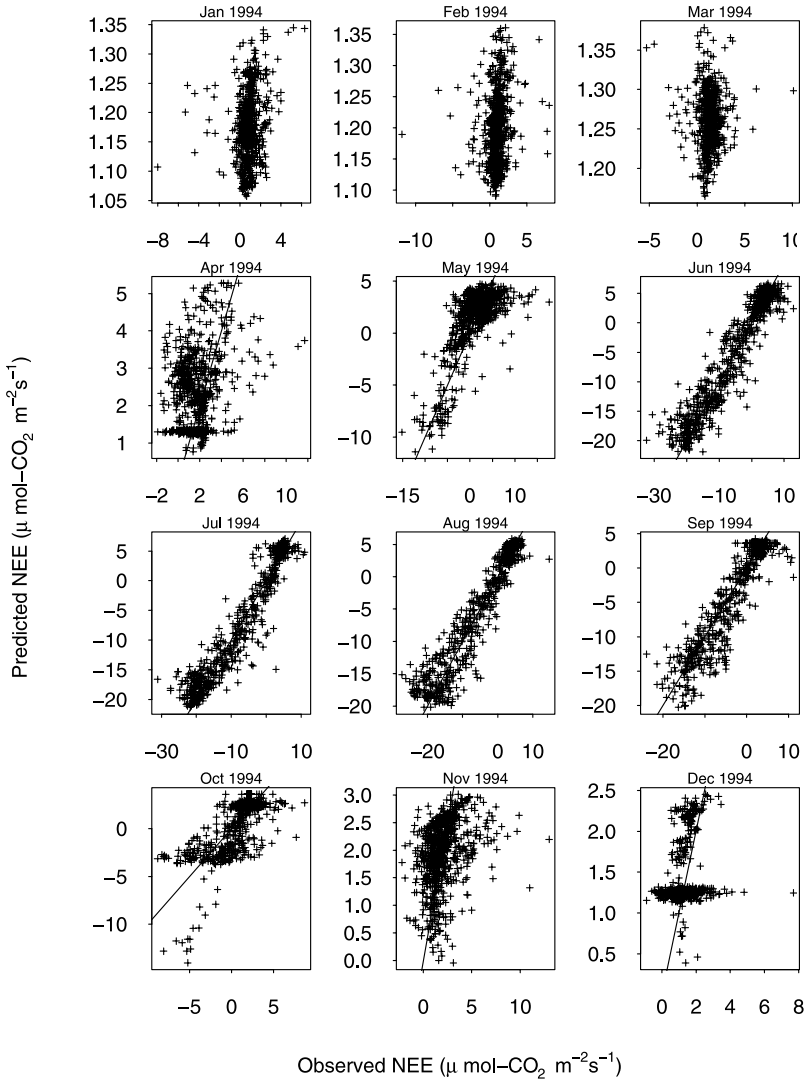

Figure 7. Scatterplots of predicted and observed hourly NEE at the HFEMS tower shown for each month of the year 1994. The lines are 1:1 lines. Predictions are poorly correlated to observations in winter months, but track each other closely in June–August. Similar patterns were observed in the other years. NEE in units of μmole CO_2 m^{-2} s^{-1}.

indicating that agreement between the IBIS-2 annual mean and the observations is coincidental. The efflux predicted by IBIS-2 in the dormant season is below the observed R, by 1.4 Mg-C ha^{-1} yr^{-1} on average, offset by positive bias in growing season R (1.7 Mg-C ha^{-1} yr^{-1}). The amplified seasonal cycle in IBIS-2 (Figure 14b) indicates excessive response of R to temperature in the model.

[42] IBIS-2 predicts winter soil temperatures much colder than observed (as much as −3.5°C [*Kucharik et al.*, 2006]), a major reason for the underestimate of R in the dormant season. IBIS surface soil temperatures drop below 0°C for much of the winter, in contrast to observations which indicate temperatures typically 1°–2°C above freezing [*Kucharik et al.*, 2006] due to insulation by snow. IBIS heterotrophic R is effectively zero in the midwinter and autotrophic R is extremely weak. Hence the sophisticated treatment of soil in IBIS-2, including explicit carbon pools and detailed 8-layer soil submodel, is no better than Model-0 for predicting the hourly, monthly, or seasonal-scale variability in R during the dormant season, and Model-0, by design, has better mean values. Physical processes such as depth and porosity of snow [*Musselman et al.*, 2005; *Sommerfeld et al.*, 1996], presence of ice layers and frozen soil [*van Bochove et al.*, 2001], and short-term variation driven by winds [*Takagi et al.*, 2005] that are not simulated in the model, may be important contributors to variability of NEE in the dormant season.

[43] Springtime canopy development is premature in IBIS compared with in situ LAI and phenological observations [*Kucharik et al.*, 2006], resulting in spring GEE roughly 1 Mg-C ha^{-1} greater than the observed. In principle, bias from using a fixed phenology could be corrected by driving the model with variable phenology derived from observations, at the sacrifice of predictive capability. Prediction of phenology appears to be a general problem for all ecosys-

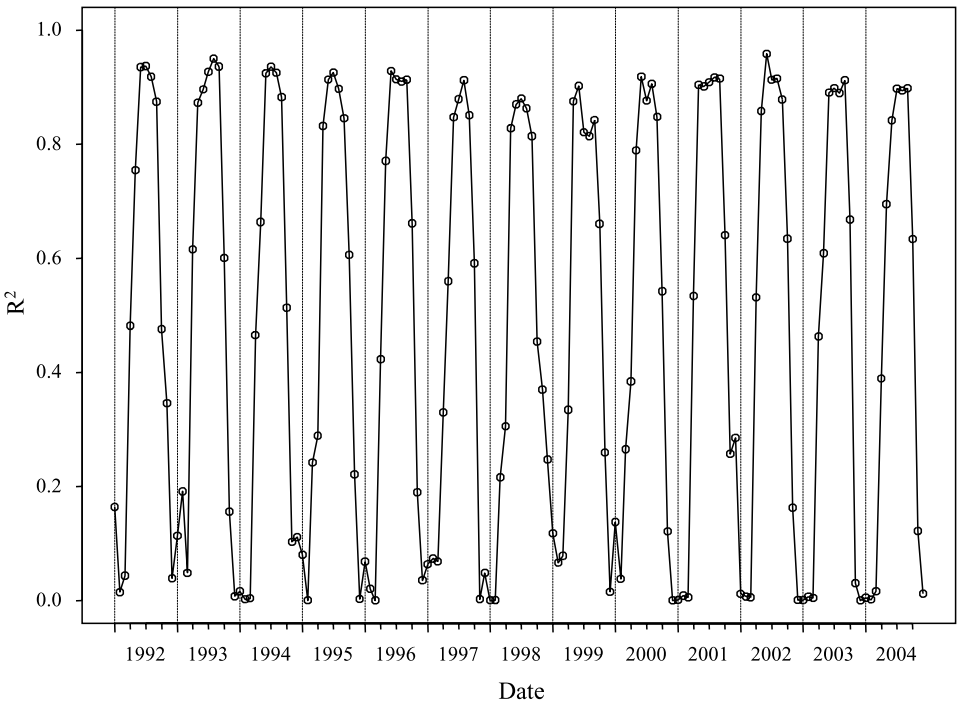

Figure 8. Coefficient of determination between Model-0 predicted and observed NEE at HFEMS for monthly averages. R^2 approaches 0.9 in the summer months, but drops to nearly 0 in the winter.

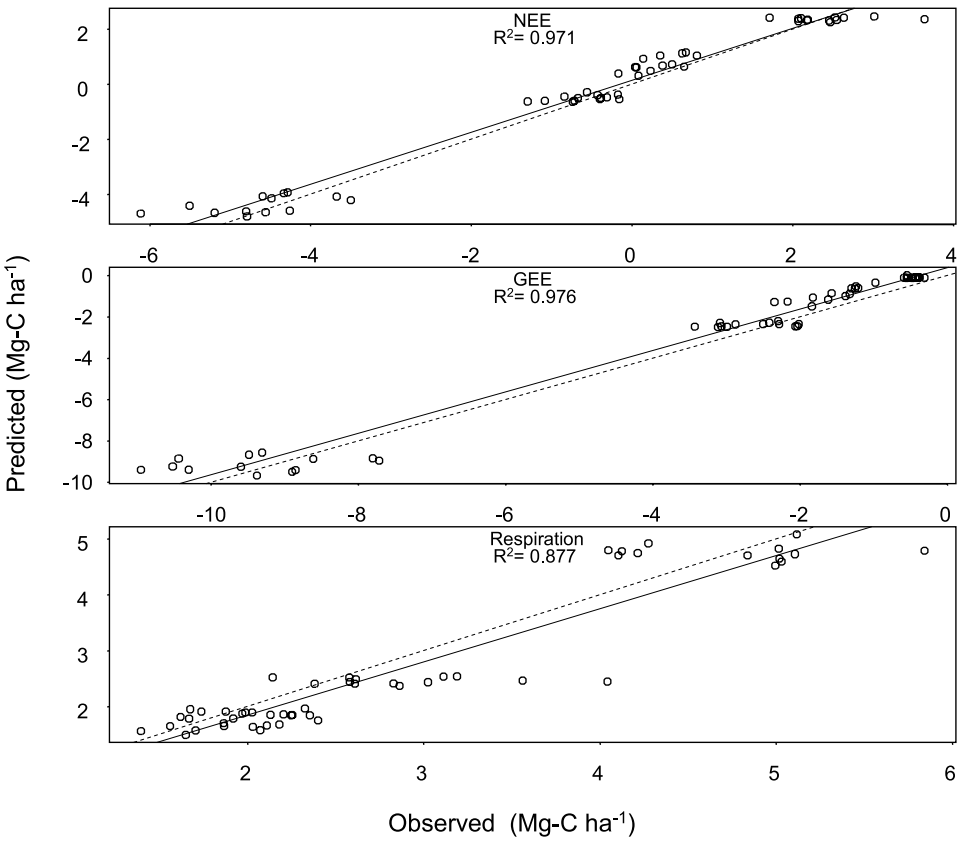

Figure 9. Seasonal sums of NEE, GEE, and R predicted by Model-0 are compared to observations. Dashed lines are 1:1 line. The solid line is the least squares fit. Overall the predictions match the observation, but within any one season there is considerable scatter.

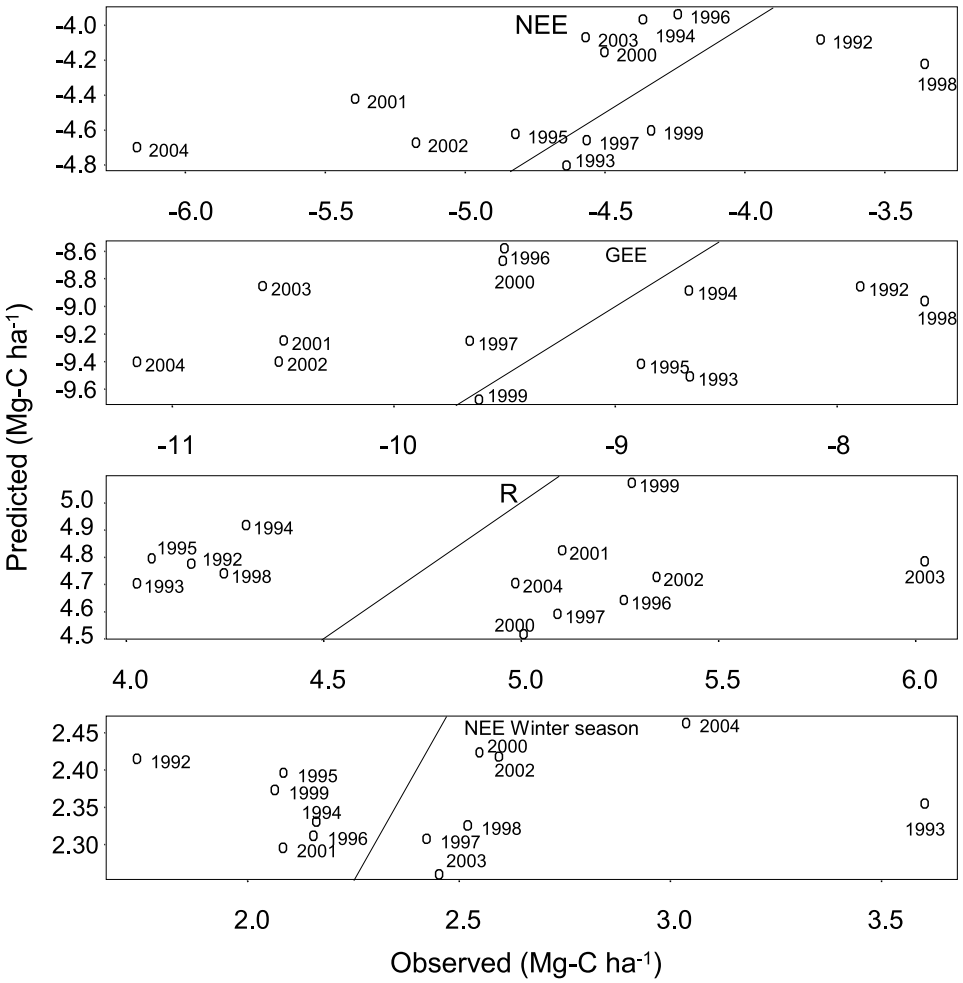

Figure 10. Model-0 predicted and observed NEE, GEE and R for summer seasons are shown in the top three plots. Model-0 predicted and observed NEE in the winter is shown in the bottom plot.

tem models, and our data show that the implications for carbon cycle simulations are quite large.

3. Discussion

[44] During the growing season, physiological responses to weather were the dominant factors contributing to variance in net CO_2 exchange. Strong dependence of GEE on light overwhelmed other sources of variance, and a simple statistical model described NEE variability well, even though variations in R were poorly simulated. Weather-driven variance of NEE and GEE dominated total variance for hourly, monthly, and seasonal timescales. Variations in annual sums of NEE were caused by year-to-year differences in GEE, with the exception of a notable anomaly in 1993 [*Goulden et al.*, 1996a]. IBIS-2 also produced rela-

Table 4. Model-0 Predicted NEE Versus Observed NEE for Season Timescale[a]

Season	N	<obs>	MAE	RMSE	a0	a0.se	a1	a1.se	r	R^2
Late fall	9	1.93	0.35	0.47	6.80	2.61	−2.59	1.39	−0.576	−0.306
Winter	9	1.22	0.24	0.32	17.57	12.01	−13.4	9.84	−0.458	−0.032
Early spring	9	1.26	0.28	0.32	0.32	0.86	0.71	0.64	0.388	0.125
Late spring[b]	9	−0.90	0.48	0.70	−0.28	0.21	0.62	0.13	0.879	0.482
Early summer	9	−5.13	0.38	0.46	0.37	1.53	1.07	0.29	0.808	0.651
Midsummer	9	−4.10	0.58	0.65	0.01	2.24	1.03	0.56	0.572	0.327
Late summer	9	−1.76	0.55	0.73	−1.28	1.07	0.26	0.55	0.177	−0.215
Early fall	9	0.83	0.19	0.23	0.18	0.48	0.85	0.63	0.452	0.198

[a]Data are based on 5-day aggregates (see text). Statistics are based on intercomparison Model-0 with observations for DOY 301, 1991, through DOY 300, 2000. Seasons are the phenologically defined seasons used in Model-0 development and analysis; see Appendix C. N is number of valid observations used in calibration. Unit of <obs>, MAE is μmole CO_2 m^{-2} s^{-1}; <obs>, mean of observations; RMSE, root mean square error; MAE, mean absolute error; r, correlation coefficient; $R^2 = 1 - \frac{\mathrm{var}(residuals)}{\mathrm{var}(obs)}$. Here a0 and a1 (a0.se and a1.se) are intercept and slope (standard error) for linear regression of Model-0 NEE versus observed NEE (NEE_{obs} = a0 + a1*NEE_{pred}).

[b]Late spring data obtained using PRI (see text and Appendix C).

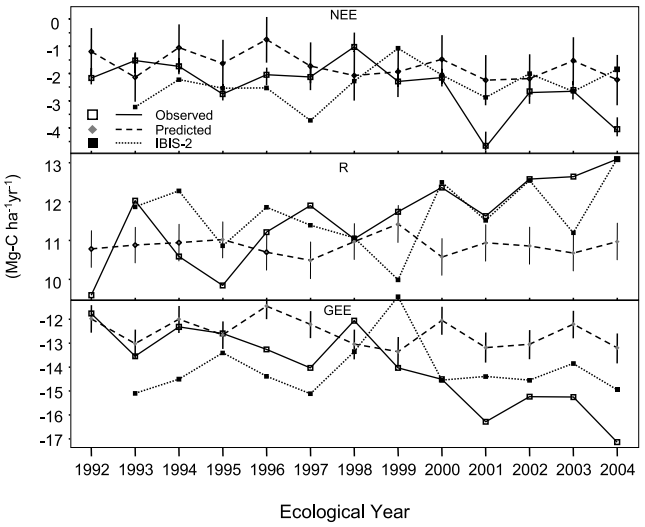

Figure 11. Annual sums of observed and predicted NEE, R, and GEE at the Harvard Forest EMS. Annual sums are computed for "ecological" years, that are selected to start on the approximate date when photosynthesis ends in the fall (DOY 300). The solid line with black squares indicates the observed annual NEE, with 95% confidence intervals as in Figure 2. The dashed line with diamonds indicates the annual sums predicted from Model-0. Vertical segments show the 90% confidence interval for the predicted values based on generating 1000 predictions using model parameters drawn from a Gaussian distribution around the computed coefficients. Annual sums predicted from the IBIS-2 model are shown by the solid line with solid square markers.

tively good agreement with GEE observations during the growing season, but its incorrect values for R caused NEE to be too positive (too little uptake). Phenology and soil moisture explained some additional variance. Despite expectations that moisture would be an important factor predicting variability in NEE, it was important only during midsummer periods. At other times of year this ecosystem apparently has sufficient access to water to prevent moisture stress from affecting canopy photosynthesis.

[45] Surprisingly, soil moisture did not affect ecosystem respiration. The response of soil respiration at small spatial scales to changes in soil moisture depends on the initial state: Wet soils respire more as they dry out, whereas dry soils respire less [*Savage and Davidson*, 2001]. Flux tower measurements aggregate over a large heterogeneous footprint, and responses by wet and dry soils in the tower footprint appear to compensate, leaving no observable response.

[46] Perhaps more surprising, within a season, R also failed to correlate to changes in temperature (soil or air), possibly likewise reflecting differing responses from different parts of the ecosystem. Variability of respiration was poorly predicted at all timescales and in all seasons, except spring, by both IBIS-2 and Model-0. Over the seasonal cycle temperature is a predictor of R, but of course many other components of the ecosystem such as active biomass [*Davidson et al.*, 2006] and pools of labile detritus are also changing. Evidently temperatures in the ecosystem cannot be taken as the direct driver of R, as often used by models. It is important to note that the poor simulation of R accounts for the difficulty in simulating interannual variations of NEE.

[47] We note that for IBIS-2, poor simulation of R was partly due to (1) the functional form and/or parameterization of R dependence on temperature, and (2) poor simulation of soil temperatures in both summer and winter. Hence, despite explicit representation of carbon pools and land-surface physics (including snowpack), IBIS captures little of monthly or longer timescale variability of R. Failure to capture the variability of dormant season R suggests that the representation of soil respiration in IBIS-2 (as in Model-0, and most models of terrestrial ecosystem carbon exchange) is flawed

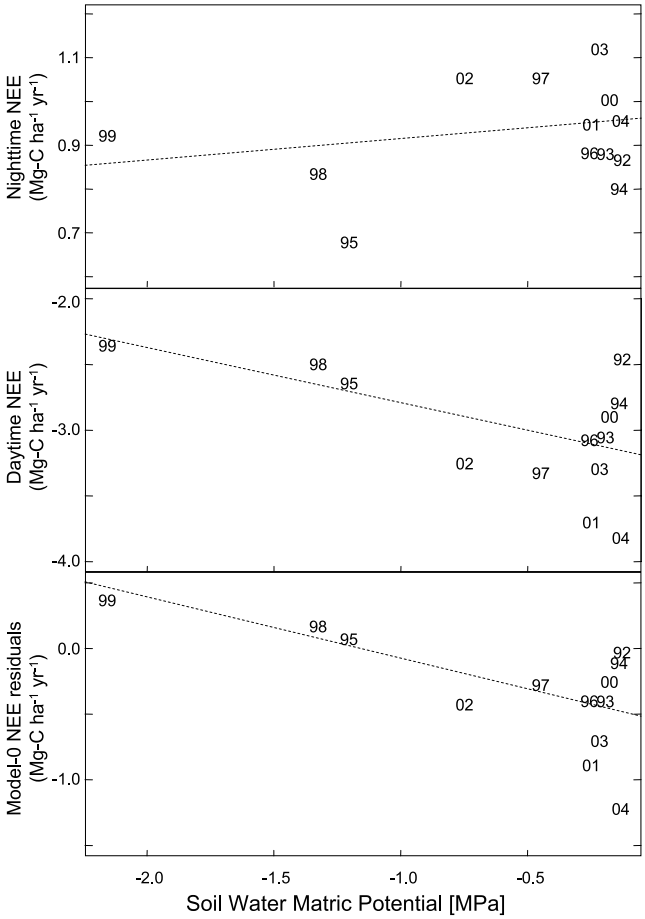

Figure 12. Midsummer (DOY 206–250) NEE and Model-0 NEE residuals versus simulated midsummer mean soil water matric potential. YY markers denote year (e.g., 99 = 1999). NEE is in units of Mg-C ha^{-1} yr^{-1}; matric potential is in units of MPa. (top) Observed nighttime NEE. (middle) Observed daytime NEE, $R^2 = 0.32$, $t = -1.55$; the correlation is statistically significant at the 90% confidence level. (bottom) Model-0 NEE residuals (observed – predicted), $R^2 = 0.45$, $t = -2.42$; the correlation is statistically significant at the 95% confidence level. Soil water matric potential was estimated using the bucket hydrology model simulated volumetric soil moisture and water retention curves for Harvard Forest [*Savage and Davidson*, 2001].

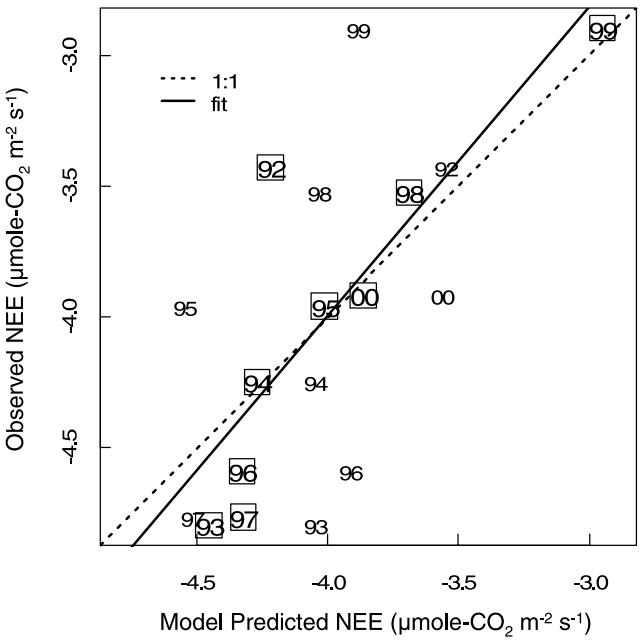

Figure 13. Midsummer (DOY 206–250) Model-0 NEE predictions with and without soil moisture drivers, compared to observed NEE. YY markers denote year (e.g., 99 = 1999). NEE in units of μmole CO_2 m^{-2} s^{-1}. Markers in squares are Model-0 predictions with soil moisture driver (Model-0c, section 1.2.2, equations (2) and (3)). The solid line is obtained from a linear least squares analysis of Model-0c NEE versus observed NEE. Best fit $R^2 = 0.71$ with a slope of 1.17 and an intercept of 0.70 μmoleCO_2 m^{-2} s^{-1}. Linear least squares analysis of Model-0 predicted NEE without soil moisture drivers yields a best fit $R^2 = 0.18$. The dashed line is 1:1 line.

and may hamper the ability of terrestrial ecosystem models to simulate accurately changes in carbon stocks for climate-change scenarios.

3.1. Seasonality

[48] The date of canopy development varies by up to 3 weeks in the spring, an important factor for annual carbon exchange. No trend was been observed in spring canopy development at Harvard Forest, but a trend in the growing season end date (defined by the fall inflection in the NEE cumulative sum curve) did emerge. From 1992 to 2004, the end of the growing season was delayed 1 day yr^{-1} ($R^2 = 0.70$, $p < 0.05$), accompanied by an increase in October net uptake that accounts for ~15% of the trend in annual CO_2 sequestration (0.3 Mg-C ha^{-1} of 1.9 Mg-C ha^{-1} from 1992–2004; see Figure 2). Our data are insufficient to distinguish whether the shift in termination of uptake is due to delayed senescence or to overall increased canopy photosynthetic capacity.

3.2. Photosynthetic Capacity

[49] Canopy light use efficiency increased significantly, and steadily, over time, punctuated by a disturbance event in 1998 that lasted until 2001. Figure 15a (see Figure 4) shows this trend, measured by GEE at near-saturating light levels. The observed pattern corresponds in part with the trend of increasing LAI after 1998 (Figure 4), but LAI apparently reached a plateau while photosynthetic capacity continued to increase. Canopy data (LAI, foliage lignin and nitrogen content (S. Ollinger, University of New Hampshire, personal communication, 2004)) suggests the low GEE observed in 1998 may be linked to ecological stress or trauma that damaged the foliage or retarded canopy development, and in situ measurements of LAI show the canopy development was stunted in early June (Figure 15c).

[50] Several events in 1998 could have damaged the canopy. The snow cover in 1998 was scant, allowing deeper frost penetration; there was a widespread ice storm in the winter of 1998 although severe damage was not apparent in the vicinity of Harvard Forest; the spring was warm and canopy development commenced in mid May, followed by a frost event with nighttime minimum temperature of −2°C on 5 June; severe thunderstorms passed through the area on 30–31 May, with 56 mm of rain observed at Harvard Forest, and reports of hail and damaging winds in nearby towns; and finally, the remainder of June was unusually cloudy and rainy, with the lowest total sunlight for June of any year in the data. We cannot directly attribute the apparent damage to the canopy to any one or combination

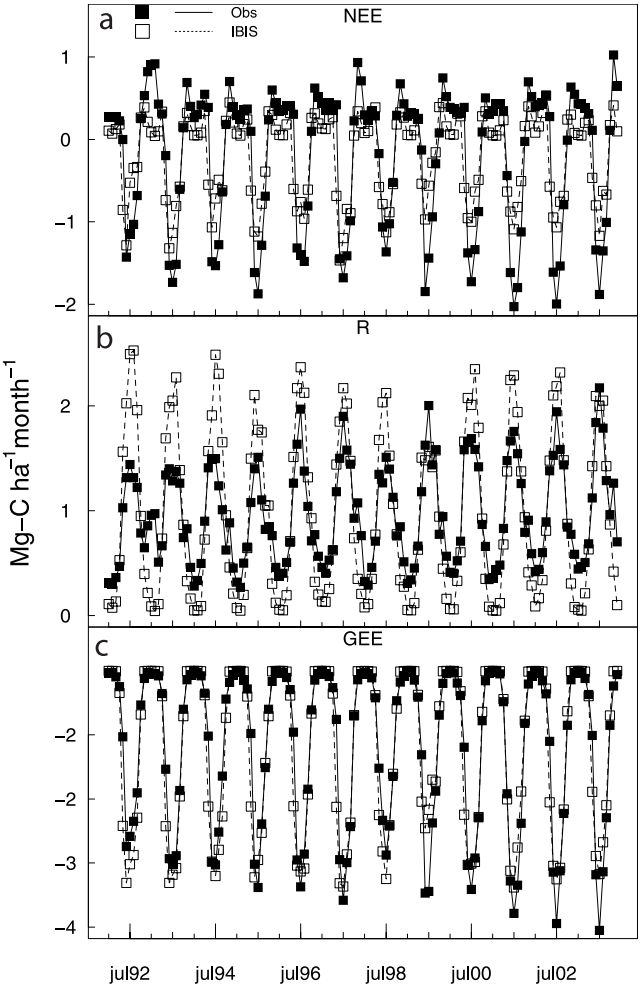

Figure 14. Monthly averages of (a) NEE, (b) R (b), and (c) GEE are shown for IBIS-2 predictions (open symbols with dashed line) and compared to observations (solid symbols).

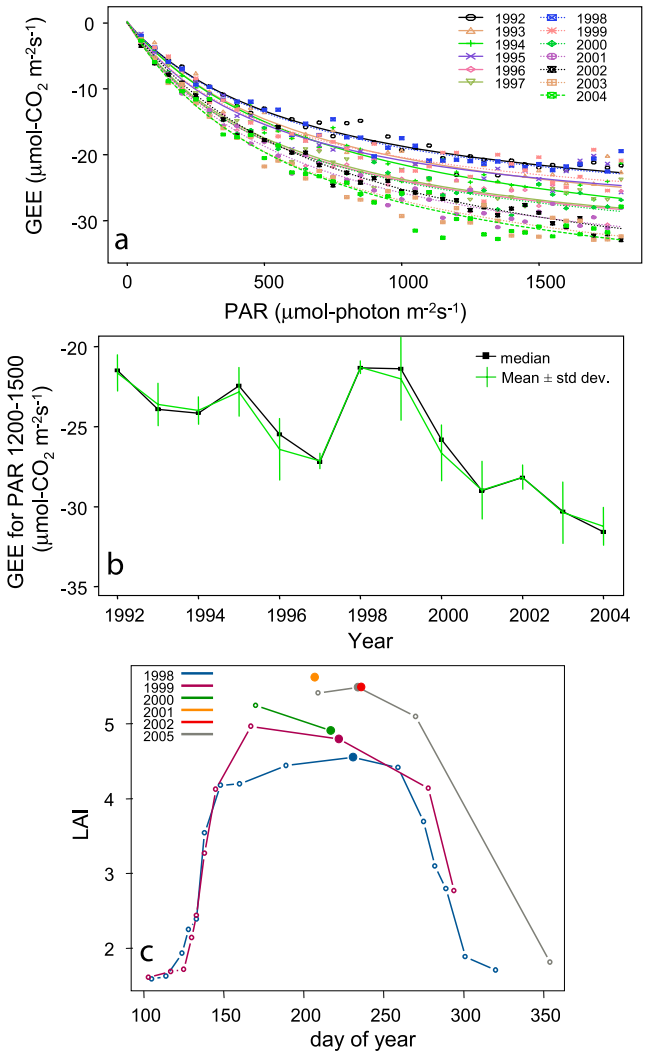

Figure 15. (a) GEE versus light curve during the month of July for each year (1992–2004) at the HFEMS. Symbols show the average GEE and PAR within 50 μmole $m^{-2}s^{-1}$ PAR bins. (b) Mean and median GEE for each year 1992–2004 within the window of optimum PAR (1250–1500 μmole $m^{-2}s^{-1}$). Note the steady trend toward increased photosynthetic uptake, punctuated by an anomaly in 1998, and recovery over the following two years. (c) Seasonal pattern of LAI at the HFEMS plots. LAI is similar up to day 150 in 1998 (blue line) and 1999 (red line), after which it continues to increase in 1999, but not in 1998. LAI at the BigFoot plots was only measured once or twice per year in the midsummer during 2000–2002 [*Gower*, 2004]. Solid symbols highlight the observations that were selected to show in Figure 4.

of these events, but it is clear that some disturbance event(s) retarded canopy development, and this event had a legacy of decreased canopy photosynthetic capacity for at least two years. A rebound (i.e., release of stronger trees) from this event may have contributed to increased photosynthetic capacity and GEE in 2001 and beyond. An important corollary of 1998 events is that weather anomalies occurring at sensitive times can have disproportionately large and long-lasting impacts on the capacity for carbon uptake in a forest ecosystem. This is an important issue when deciding how long eddy-covariance towers need to be emplaced to measure ecosystem mean properties; clearly predictions of carbon budgets should consider not only mean climate, but also the variability and probability of extreme weather events.

3.3. NEE and Growth

[51] Comparisons of NEE and AGWI indicate a 1-year lag between uptake and tree growth. Years with peak carbon uptake (2001, 2004) directly precede years of peak AGWI (2002, 2005). This behavior is not unexpected, since carbohydrates stored during favorable growing seasons are used the following year to support growth [cf. *Barford et al.*, 2001]. However, the observed lag is notably shorter than the 3–6 years reported by *Krakauer and Randerson* [2003] for tree rings to respond after volcanic eruptions.

3.4. Long-Term Trends, Disturbance, and Anomalies

[52] A goal of this analysis was to partition the source of specific carbon exchange anomalies into climatic versus ecological driving factors. For example, the magnitude of growing season GEE in 1998 was 1.9 Mg-C ha^{-1} below the 13-year mean, leaving a deficit in NEE of +1.3 Mg-C ha^{-1}, in spite of early canopy emergence in the spring and below average ecosystem R for the year (−0.5 Mg-C ha^{-1}). Model-0 analysis indicates about half of the early summer NEE anomaly (0.4 of 0.7 Mg-C ha^{-1}) could be attributed to low insolation and cool temperatures. The balance of the deficit in growing season uptake was a consequence of reduced photosynthetic capacity: in the late spring, GEE and net uptake were significantly less than anticipated on the basis of PAR, temperature, and canopy development (Figure 15), and photosynthetic efficiency continued below-average throughout the growing season. As noted above,

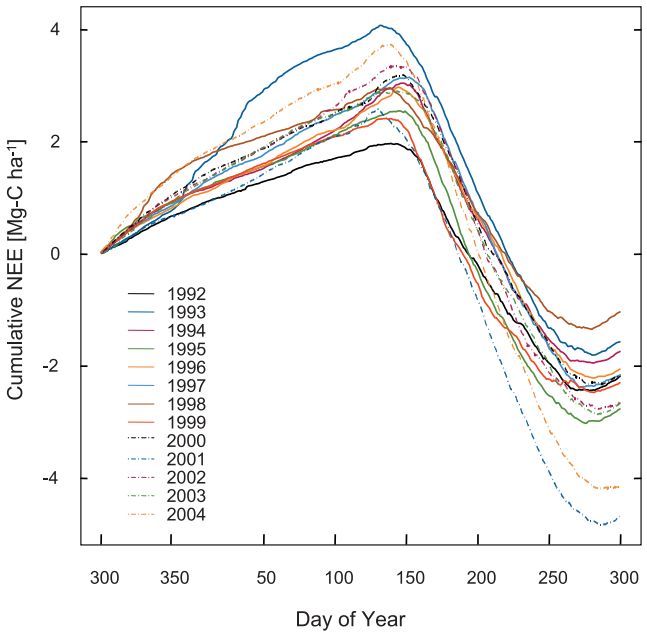

Figure 16. Cumulative NEE for each ecological year (1 November to 31 October), November 1991 to October 2004.

this anomaly is associated with anomalies in many other parameters, and appears to reflect a disturbance event with a significant legacy.

[53] In 2001, net carbon uptake by Harvard Forest was nearly twice the 13-year mean. R was near average in 2001, and prior to canopy emergence, the cumulative sum of NEE was near the 13-yr mean (Figure 16). Thus GEE in the growing season alone accounts for the anomaly. Canopy development in 2001 was the earliest (Figure 16) and the start of the growing season was 9 days earlier, relative to the 13-year mean (defined by inflection point in cumulative NEE trace). The 2001 snowpack was unusually deep and persisted late into the spring. The onset of warm weather melted the snow quickly, and absence of soil frost allowed the soil to drain and warm quickly.

[54] Even though the late spring of 2001 was the most productive of the study period, the early canopy development and favorable spring weather conditions were responsible for only ~20% of the anomalous annual NEE observed in ecological year 2001 (0.5 of 2.2 Mg-C ha^{-1}). Anomalously high GEE, average R, and the resulting high net uptake, continued throughout the growing season, with CO_2 uptake exceeding the 13-year mean by nearly 40% (1.70 Mg-C ha^{-1}). Model-0c captures about 40% of the 2001 anomaly with the combined effect of early growing season onset, favorable summer weather conditions, and extended duration of the growing season (~0.9 of 2.2 Mg-C ha^{-1}). More than half of the anomaly appears to be due to ecological and/or environmental factors that increased canopy photosynthetic efficiency (Figure 15b).

[55] Many anomalies in NEE observed at HFEMS between 1992 and 2004 were correlated with climate anomalies, but Model-0, giving the mean ecosystem responses to temperature, light, moisture, and seasonality, could account for only 40–50%. Evidently interannual responses of NEE are significantly driven by changes in the underlying physiology of the ecosystem, which itself responds to climatic factors.

[56] Significant long-term trends of increasing NEE, GEE and R are apparent in the HFEMS flux data, and the Model-0 analysis indicates that these trends are not driven by decadal-scale trends in climate or growing season length, as in the case of annual anomalies. Instead, the trends in NEE, G, and R appear to reflect fundamental changes in the ecosystem over the past 13 years. The increased uptake of CO_2, most pronounced since 2000, was clearly associated with increased leaf area and canopy photosynthetic capacity. The acceleration of uptake since 2000 is especially surprising given the age (75–110 years), composition (northern red oak, red maple), and rather poor soils at this site. Most silvicultural tables would predict slowing of forest growth, based on increasing competition for limiting resources in the stand, or on limitations of hydraulic conductivity with respect to the size of individual trees. Decreasing net productivity in mature stands is often postulated to follow when LAI reaches a maximum, because respiration costs of tissue construction and maintenance continue to increase as trees grow [cf. *Waring and Schlesinger*, 1985]. Although we cannot be sure that LAI at HFEMS will not increase further, the observed plateau suggests that the maximum has been reached (Figure 4).

[57] Other explanations must be sought to explain the crucial and surprising increase in canopy photosynthetic capacity (> 50% larger now than in 1992). A protracted rebound from the disturbance of 1998 would not explain the trend since 1992. We think that the potential for growth and accumulation of carbon for this type of Northern ecosystem may be greater than previously thought, as suggested by *Medvigy* [2006]. The increasing dominance and basal area of Northern Red Oak at the site is clearly a factor, related to long-term succession: red oak photosynthetic capacity is twice that of red maple [*Bassow and Bazzaz*, 1997]; red maple is the second most abundant tree. Simple scaling of HFEMS uptake by this factor, weighted by the increase in red oak in the forest, is sufficient to explain the observed trend of NEE and GEE. We also cannot rule out some growth acceleration in response to rising CO_2, and possibly other factors such as nutrient inputs.

4. Conclusion

[58] The HFEMS long-term eddy-flux and biometry study shows that the short-term (hourly, monthly) rates of ecosystem photosynthesis are closely linked to light and temperature, consistent with expectations from leaf-level studies. Water stress has unexpectedly small impact on this ecosystem, restricted to the late summer in dry years. Limitations of water supply to the canopy are small, but evident throughout the growing season, and our matric potential model links this effect to stem and/or root conductance, rather than VPD or restricted soil moisture. Within a season, ecosystem respiration does not respond to temperature, also an unexpected result that may reflect the heterogeneity of the temperature response for respiring components of the forest.

[59] NEE exhibits significant interannual variability, due to variations in GEE. Clearly several years of data are needed just to define the mean rates of carbon exchange or to quantify mean responses to climate variability. With 13 years of data we were able to identify disturbance-related anomalies and their legacies, and to measure the underlying trends toward greater rates of net uptake, increased photosynthetic capacity, and higher rates of ecosystem respiration. These trends are surprising given the age of the forest. Changes in growing season length or similar climatic trends appear not to be primary driving factors. Likewise, current ecosystem models do not appear to capture the long-term aspects of the data. The notable increase in red oak AGWB could account for most or all of the acceleration of uptake and enhancement of canopy efficiency. The course of succession at the site could possibly have been influenced by recovery from gypsy moth defoliations in the 1980's, since the oaks were preferred by the caterpillars, but if recovery from that disturbance were the main driver, we would expect to observe more response early in the record, rather than at the end.

[60] The forest stand age at which CO_2 uptake slows down, creating a carbon steady state is one of the most important factors determining the total magnitude of the future forest sinks of atmospheric CO_2. It may seem unlikely that the trend of the last 13 years could continue for a long time, allowing Harvard Forest NEE, GEE and R to approach values previously found only at lower latitudes. Classical ecosystem dynamics and carbon-accounting models [*Houghton et al.*, 1983] predict that the forest carbon

uptake should soon decline, and eventually GEE will be balanced by respiration (NEE = 0 [e.g., *Gower et al.*, 1996; *Ryan et al.*, 1997]), or overbalanced by increasing maintenance respiration.

[61] The current results call these accepted ideas into question. Possibly Northern forests have greater than the expected capacity to take up CO_2 over the long term. We do not have suitable examples of old forests of this type, in current climate, to predict how long we can expect the forest to continue accumulating carbon, how much can be accumulated in total, or how long accumulated carbon will remain sequestered. In order to predict the course of forest carbon sequestration, better understanding of tree life histories, land use and disturbance history, and detailed knowledge of resource limitation in many types of stands are required. There is little doubt that succession is playing a role in the increased carbon sequestration in this forest, while climate change appears to be much less important. The combination of flux data over long periods with long-term data sets on stand structure, dynamics, allocation and growth, appear to offer the most potent tools for assessment of these questions.

[62] Recent observations of growth increase in long-term tropical forest plots [*Baker et al.*, 2004; *Lewis et al.*, 2004] have raised similar questions, with several possible explanations (e.g., recovery from ENSO disturbances, increased CO_2, changing light regime), but no dominant rationale. This will evidently be a key factor in predicting the future role of forests in the global carbon cycle.

Appendix A: Climate Drivers

[63] Supplemental climate data, comprising daily precipitation totals, snowfall, and minimum and maximum air temperature have been obtained from the Shaler and Fisher meteorological stations (http://harvardforest.fas.harvard.edu/hfmet/) (located 1500 m from the tower and station) and several surrounding weather stations [*National Climatic Data Center*, 2006]. Hourly and daily precipitation and cloud cover data from Orange Airport (<10 km N-NW from tower) for April 1995 forward have also been used [*National Climate Data Center*, 2006].

A1. PAR

[64] When available, gaps in the hourly above-canopy PAR data set were filled using PAR measurements taken on the HFEMS tower by the ASRC–SUNY research group. For periods in 2001–2004 when measurements are not available from either the Harvard or ASRC PAR instruments, the hourly global solar radiation measurements or PAR from the Fisher meteorological station (operational in February 2001) were used to estimate above-canopy PAR at the HFEMS site. In December 2003 a PAR sensor was added to the Fisher meteorological station and missing PAR observations are replaced with Fisher station data directly. When the ASRC and Fisher radiation data are included, only 1145 hours of PAR observations are missing for the entire November 1991 to December 2004 time period. These remaining gaps in hourly PAR data were filled using the mean diurnal PAR cycle for a 30-day window centered on the day with missing data.

Table A1. Names and Locations of Meteorological Stations Providing Data to Estimate Daily Precipitation at HFEMS When Measurements at the Shaler or Fisher Meteorological Stations Were Unavailable

Station Name	Station Identification	Latitude	Longitude
Orange	54756	42.567	−72.283
Tully Lake	198573	42.633	−72.217
Birch Hill Dam	190666	42.633	−72.117
Gardner	193052	42.583	−71.983
Barre Falls Dam	190408	42.433	−72.033
Hardwick	193401	42.350	−72.200
New Salem	195306	42.450	−72.333

A2. Air Temperature

[65] Missing hourly measurements in the 27 m and 2.5 m air temperature data set were filled using appropriately adjusted measurements from adjacent levels in the air temperature profile, the sonic anemometer, or the Fisher meteorological station. Prior to the establishment of Fisher meteorological station, when profile or sonic anemometer data was unavailable, the daily mean air temperature measured at Shaler meteorological station and the 10-year mean diurnal temperature cycle for a 30-day window centered on the day with missing data were used to estimate missing hourly air temperatures.

A3. Precipitation

[66] Daily precipitation totals were obtained from the Fisher and Shaler meteorological station records. Missing data in the Fisher and Shaler precipitation records was filled using a distance-weighted average of several surrounding meteorological stations [*National Climate Data Center*, 2006]. Station locations are given in Table A1.

Appendix B: Gap Filling and Time Integration

[67] Equipment failure and data rejection reduce the average annual data coverage of our continuous eddy covariance measurements of NEE to about 50%, a fraction typical of continuous eddy covariance measurement sites [*Falge et al.*, 2001a]. A malfunctioning data acquisition system resulted in the loss of canopy CO_2 storage data for two extended periods in 1997 and 2002, while occasional malfunctioning of the CO_2 profile sampling system created additional, shorter duration gaps in the canopy CO_2 storage data set. For periods lacking canopy CO_2 storage data, hourly NEE (NEE = FCO_2 + change in canopy CO_2 storage) was derived by summing FCO_2 observations with a seasonally varying, hourly mean storage term.

[68] Three variants of time integration algorithms: nonlinear regression, look-up tables, and diel mean cycle [*Falge et al.*, 2001a], were used to estimate monthly, seasonal and annual sums of NEE, R, and GEE. The nonlinear regression technique is based on combining a Van't Hoff function for temperature dependence of respiration with a Michaelis-Menten function to account for photosynthetic response to light. Observations of NEE, PAR and air temperature (T) were used to optimize the equation parameters for approximately 30-day periods, and missing observations of NEE were estimated using the optimized equation. The look-up table method divided the data set into approximately two-month periods and classified observations of NEE accord-

ing to PAR and T. For each period, observed NEE was averaged according to class, creating a table from which missing NEE observations could be estimated on the basis of environmental conditions (PAR and T). The diel mean cycle method divides NEE data into 5-day blocks within a 15-day window. Valid NEE observations were averaged by hour of the day, and missing NEE data for the 5-day block were estimated using the mean for the appropriate hour. If needed the 15-day window was expanded to ensure at least 3 valid NEE data for each hour of the 24 hours.

[69] None of the three methods exhibited a relative bias in annual sums. The simple average of the three time integration methods yields uncertainties in NEE annual sums which are lower than that of any single individual method. We have chosen the three-method average as the best estimate of time integrated NEE, R, and GEE.

[70] Random sampling of the NEE error populations was used to determine the uncertainties in annual sums of NEE. Each ecological year was divided into 12 periods (6 seasons, day and night). Uncertainties for gap filled hours were estimated by randomly drawing from the error population defined by hours with valid NEE observations ($NEE_{observed} - NEE_{estimated}$). The mean difference between observations and estimates was 0. The uncertainties for valid hourly NEE observations were estimated by randomly drawing errors from a double exponential probability distribution with shape factors for daytime and nighttime measurements from *Richardson et al.* [2006]. For each ecological year, 3000 simulations were used to define the 95% confidence intervals reported for the annual sums of NEE.

B1. Nonlinear Regression

[71] Nonlinear regression techniques typically involve the use of a temperature function [*Lloyd and Taylor*, 1994] and a light response curve [cf. *Falge et al.*, 2001a], representing ecosystem respiration and photosynthetic carbon assimilation, respectively. For gap filling daytime hours we have employed the sum of a Van't Hoff function (term 1, equation (B1)) and a Michaelis-Menten function (term 2, equation (B1)), while the gap filling of nighttime hours used a Michaelis-Menten function alone (i.e., set term 2 in equation (B1) = 0).

$$NEE = a_0 * \exp[a_1(T - \langle T \rangle)] + PRI * \frac{a_3 * PAR}{a_4 + PAR}. \quad \text{(B1)}$$

[72] The complete time period from 28 October 1991 through 31 December 2004 was divided into 10-day blocks. For a 30-day window about the center of each 10-day block, valid observations of FCO_2, PAR, and T, were used in to optimize the parameters in equation (B1), which then provided an estimate of missing FCO_2 during the 10-day block. Daytime and nighttime were treated separately. During the dormant season, term 2 of equation (B1) was simplified to a linear PAR response. Respiration during the night and dormant season (DOY > 340 or DOY <61) was taken as the gap filled NEE (observed or estimated FCO_2). Daytime R outside the dormant season was estimated using term 1 of equation (B1) optimized using nighttime data. Employing FCO_2 (not NEE) to estimate R introduces a systematic bias. Daytime estimates of ecosystem respiration are based on nocturnal observations of NEE(= R).

Table B1. Calendar Year Sums of NEE, R, and GEE at Harvard Forest From 1992–2004[a]

	Annual		
Calendar Year	NEE	R	GEE
1992	−1.6	10.1	−11.7
1993	−1.8	11.8	−13.6
1994	−1.7	10.6	−12.4
1995	−2.8	9.7	−12.5
1996	−1.9	11.3	−13.3
1997	−1.6	12.4	−14.0
1998	−1.6	10.6	−12.1
1999	−2.1	11.9	−14.0
2000	−2.6	11.9	−14.5
2001	−4.3	12.1	−16.4
2002	−2.7	12.4	−15.1
2003	−2.1	13.2	−15.4
2004	−4.6	12.5	−17.1

[a]Data are in Mg-C ha^{-1} yr^{-1}.

B1.1. Look-Up Table

[73] The look-up table method [*Falge et al.*, 2001a] involved dividing the data set into approximately 2-month periods and for each period creating a table from which missing FCO_2 could be estimated on the basis of environmental conditions. For each 2-month period daytime hours were assigned to different classes of air temperature (defined on 4°C intervals) and PAR (defined on ~150 μmol m^{-2} s^{-1} intervals) while nighttime hours were classified by air temperature alone (defined on 2°C intervals). Mean values of FCO_2 were then calculated for each class of PAR and T (or T alone for nighttime observations). Gaps in the look-up tables were filled using linear interpolation. Missing hourly FCO_2 observations were filled using the appropriate look-up table. Nocturnal and dormant season (DOY > 340 or DOY <81, 7 December to 21 March) daytime FCO_2 was taken as the ecosystem respiration (i.e., R = FCO_2). Respiration during the growing season daytime was estimated using the nighttime look-up table with linear interpolation to higher temperatures.

B1.2. Diel Cycle

[74] The data set was divided into 5-day blocks and for a 15-day window about each 5-day block, valid FCO_2 observations were averaged by hour of the day. When necessary, the 15-day window was expanded to ensure a minimum of 3 valid FCO_2 observations for each hour of the day for the averaging period. Missing FCO_2 observations for a given 5-day block were estimated using the appropriate hourly mean. Windows of variable width about the 5 blocks were tested. Nocturnal and dormant season (DOY > 341 or DOY <80, 7 December to 21 March) daytime FCO_2 was taken as the ecosystem respiration (i.e., R = FCO_2). Daytime, growing season R was estimated as the mean of the gap filled, nighttime FCO_2 for a given 5-day bin; R is assumed to be independent of temperature.

B2. Nonparametric Gap Filling

[75] In order to compare temporally aggregated modeling predictions with observed NEE, we have employed a nonparametric gap filling scheme which is independent of Model-0 drivers (i.e., PAR and T, see below). Valid, u* - filtered observations of FCO_2 and canopy CO_2 storage were averaged by hour of the day according to 5-day bins, creating 5-day aggregates. Gaps in the 5-day aggregates were filled using

bivariate interpolation. Similarly, 5-day aggregates of Model-0 predicted NEE were also created, using only hours when valid, u* - filtered FCO_2 observations were available. For each 5-day aggregate of observed storage, a constant was added to each hour to ensure canopy storage of CO_2 summed to zero for that 5-day period, while preserving the diel pattern. Five-day aggregates of observed NEE were created via summation of the FCO_2 and CO_2 storage 5-day aggregates.

B3. Calendar Year Annual Sums

[76] Calendar year annual sums of NEE, R, and GEE are provided in Table B1.

Appendix C: Explanation of Model-0 Seasons

[77] The ecological year begins on 28 October (DOY 301), roughly 2 weeks after the end of the growing season (defined as the fall inflection in the NEE cumulative sum trace; see Figure 16) and runs through 27 October of the following calendar year. The significant correlation between NEE in the months of December and January was the primary motivation for our departure from calendar year. The late fall season (DOY 301–340) is the first Model-0 season of the ecological year, covering final descent of the ecosystem from the growing season into the long period of winter dormancy from early December into early April designated as the winter season (DOY 341–100). The early spring season commences shortly after the mean thaw date of the soil in the vicinity of the HFEMS tower and begins the ecosystem transition from dormant season to growing season. During the early spring season, thawing soils and daily mean air temperatures exceeding 4°C allow for the onset of regular conifer photosynthesis; the snow cover ends and canopy deciduous foliage begins to emerge. The canopy changes rapidly in the late spring when the bulk of canopy development occurs. By DOY 160 the leaf area is near the annual maximum and ecosystem is a net sink for CO_2. The period beginning with the time of full canopy development through the onset of senescence, roughly DOY 161–250, is the peak growing season. Carbon uptake reaches the annual maximum, and following a brief plateau begins a gradual decline coincident with decreasing insolation, foliar aging and the approach to minimum soil moisture. The peak growing season has been divided into the seasons of early and mid summer.

[78] The complex ecosystem transition from mid growing season into winter dormancy has been captured with 3 seasons. The late summer season coincides with the onset of senescence, signaled by the increase in canopy PAR albedo from the broad summer minimum (D. Fitzjarrald, ASRC–SUNY, personal communication, 2002; data available at ftp://ftp.as.harvard.edu/pub/nigec/SUNY_fitzjarrald/) [*Moore et al.*, 1996], typically beginning around DOY 250. The daily mean ecosystem uptake of CO_2 begins a rapid decline between DOY 250 and 260, with the ecosystem usually becoming a net source of CO_2 by DOY 280, around the time when the foliage is at peak color (J. F. O'Keefe, personal communication, 2002) and the PAR ratio starts to decrease rapidly, signifying a loss of canopy leaf area. Fifty percent of leaf fall typically occurs by DOY 300 for the dominant canopy species (red oak; DOY 285 for red maple; J. F. O'Keefe, personal communication, 2002). The early fall season runs from the later portion of the senescence period until leaf abscission is well under way (DOY 276–300).

[79] The onset of canopy emergence and rate of canopy development is highly variable from year to year, according to ground-based (J. F. O'Keefe, personal communication, 2002), and remote sensing [cf. *Xiao et al.*, 2004] phenological observations, in agreement with the PAR ratio (the midday ratio of above-canopy PAR to below-canopy PAR) measured at the HFEMS tower. The majority of canopy development occurs during the late spring and a PAR ratio index (PRI) was developed to account for interannual variability in canopy development,

$$PRI = \frac{(PR - PR_{\min})}{PR_{\max} - PR_{\min}}. \quad \text{(C1)}$$

[80] In equation (C1), PR is the daily, smoothed PAR ratio, and PR_{min} and PR_{max} are the PAR ratio prior to (DOY 90–120) and after completion of canopy development (DOY 170–205), respectively. The annual minimum and maximum PR are used to compute the PRI for each late spring, an approach that assumes the fully developed canopy is equivalent from year to year. The PRI ranges from 0 to 1 during the late spring and is set to 1 during other seasons.

Appendix D: Soil Moisture Algorithms

D1. Bucket Model of Soil Moisture

[81] Continuous soil moisture measurements over the full study period at HFEMS are not available. Soil moisture profiles have been measured at two locations in the vicinity of the EMS tower since 1997 (K. E. Savage and E. A. Davidson, personal communication, 2000). Soil water content was measured as ~6 hour averages using TDR probes inserted horizontally into the soil at 4 levels, in both well drained upland and poorly drained wetland soil plots located 150 m NW and 150 m SW of the EMS tower, respectively (K. E. Savage and E. A. Davidson, personal communication, 2000). We used these soil moisture profiles for 1997–1999 to parameterize a simple two-layer bucket-type soil hydrology model, intended to capture the relative variability of soil moisture at Harvard Forest during the growing season.

[82] This soil moisture profile data set (1997–1999) was used to parameterize a simple two-layer bucket-type soil hydrology model. The bucket model design is loosely based on the water balance methodology used to calculate Palmer soil drought indices [*Palmer*, 1965], with the soil profile divided into a shallow "surface layer" and a deep "under layer" (see Figure D1). Model simulations of surface layer and under layer volumetric soil moisture content span the growing season (DOY 100–300) with a 5-day time step. Five-day sums of latent heat flux, measured on top of the HFEMS tower, and precipitation, measured at the Shaler meteorological station, are the bucket model driving variables.

[83] Four adjustable model parameters define the water capacity of the soil, control the flux of water between the soil and the atmosphere, and regulate the transport of water from the surface layer into the under layer. Two additional model parameters control water loss from the under layer during periods of extreme water loss. The depth of the bucket model layers were fixed to match the depth of the

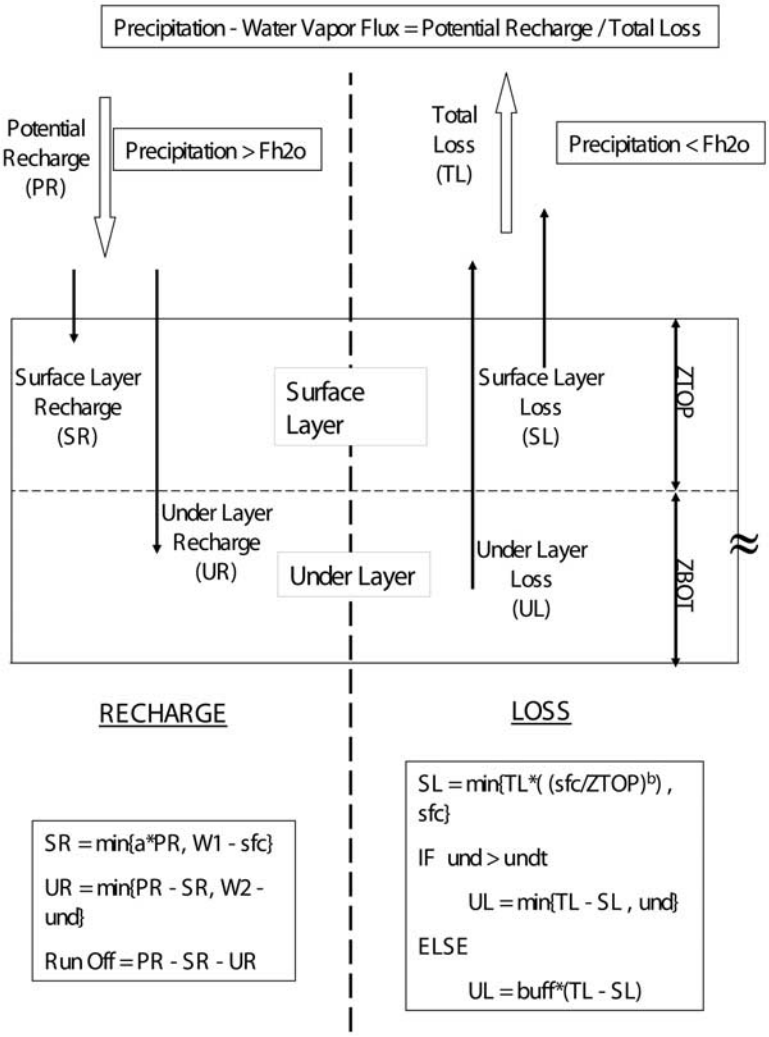

Figure D1. Schematic diagram of the soil moisture bucket model (see Appendix D).

soil moisture profiles measurement pits. The bucket model parameters were optimized to match the model-predicted volumetric soil moisture with the 1997–1999 in situ measurements of the volumetric soil moisture profile (K. E. Savage and E. A. Davidson, personal communication, 2000). An independent set of optimized model parameters was derived for each soil moisture type (well-drained soil and poorly drained soil). Parameter optimization was achieved using the genetic algorithm [*Carroll*, 1996].

[84] Optimized model parameters and calibration statistics are given in Table D1. Model predictions and observations are shown in Figure D2. The purpose of the bucket model is not to estimate absolute values of soil moisture, but to capture the relative variability of soil moisture at Harvard Forest during the growing season. The simple bucket model captures about 80% of the observed variability in the surface and under layer soil moisture during the 1997–1999 growing seasons, suggesting the bucket model is sufficient for quantifying relative soil moisture variability over the 1992–2003 growing seasons. Model simulations for the entire 1992–2003 period are shown in Figure D3.

D2. Model-0 and Soil Moisture

[85] Two modified forms of the Model-0 equation were explored in an initial investigation of the soil moisture–NEE link at Harvard Forest. The first modified Model-0

Table D1. Optimized Parameter Values and Calibration Statistics for the Bucket Soil Hydrology Model[a]

							Surface Layer			Underlayer		
	W1	W2	a	b	und	buff	r^2	a_0	a_1	r^2	a_0	a_1
Well-drained soil	24	142	0.11	1.75	70	0.20	0.75	−0.02	1.10	0.87	−0.02	1.18
Poorly drained soil	49	151	0.23	0.86	122	0.82	0.88	0.00	0.89	0.92	0.04	0.89

[a]W1, W2, a, b, undt, and buff are hydrology model parameters (see Figure D1). Parameters W1 and W2 are the maximum water content (in units of millimeters) of surface layer (W1) and underlayer (W2). Parameters a, b, buff (unitless), undt (units of mm H_2O) control water exchange; see text and Figure D1 for details. Here a0 and a1 are the intercept and slope for linear regression of the model predicted volumetric soil moisture versus the observed volumetric soil moisture (Observed = a0 + a1*Predicted) and r2 is the coefficient of determination for the regression.

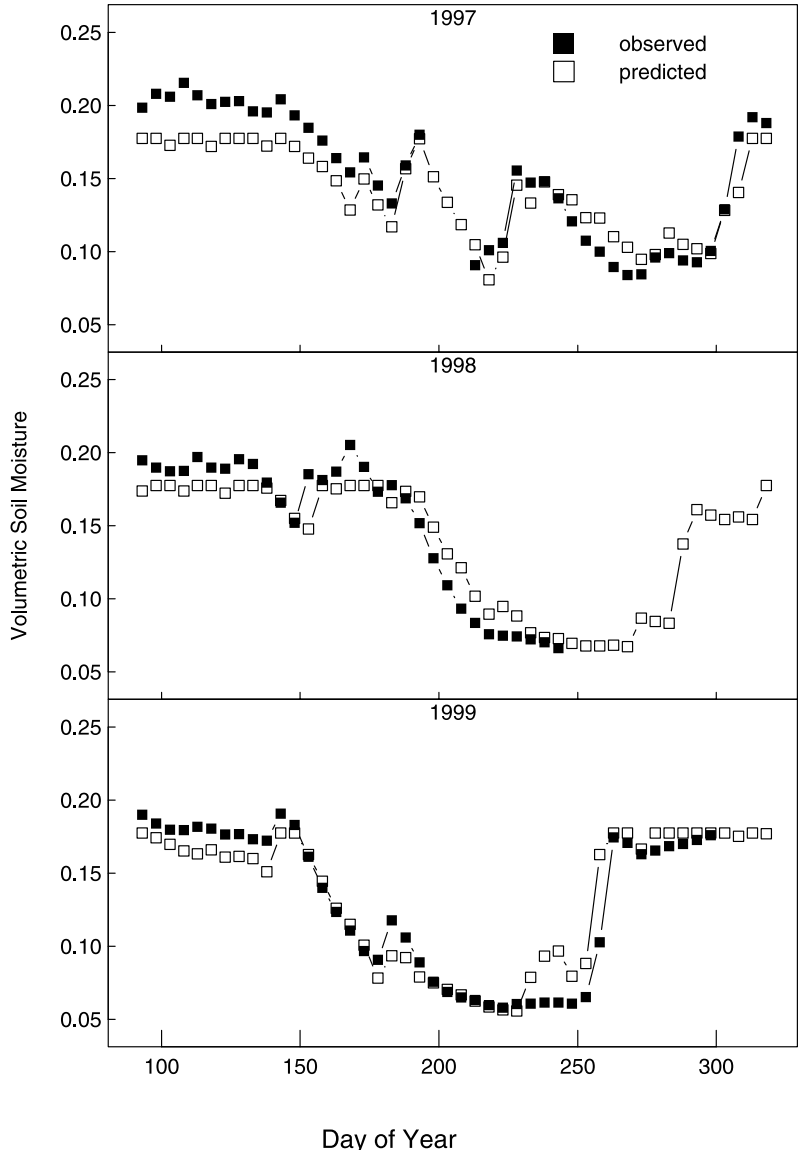

Figure D2. Calculated (open symbol) versus observed (solid symbol) [*Savage and Davidson*, 2001] soil moisture in the lower layer of the soil moisture model (see Figure D1), for years with frequent soil moisture observations. Units are mm^3 H_2O mm^{-3} soil.

equation, Model-0a, includes a function of soil moisture that may be interpreted as an additional respiration term (equation (D1)) and was designed to test for a soil moisture role in regulating ecosystem respiration. A second realization of Model-0, Model-0b (equation (D2)), multiplies the GEE term of the Model-0 equation by a soil moisture stress factor [*Foley et al.*, 1996].

[86] The modified versions of Model-0 employ volumetric soil moisture, the soil moisture measure estimated with the soil hydrology model. However, soil moisture impacts soil respiration and photosynthesis through the soil water matric potential (Ψ), which has a power law dependence on volumetric soil moisture and is expressed via soil water retention curves. Soil water retention curves have been measured for several soil plots at Harvard Forest (K. E. Savage and E. A. Davidson, personal communication, 2000), but for the initial soil moisture–NEE modeling exercise we employed exponential functions of volumetric soil moisture which mimic to some extent the $\theta - \Psi$ relationship.

$$NEE = a_1 + a_2[T - \langle T \rangle] + B + PRI^* \frac{a_3^* PAR}{a_4 + PAR}, \tag{D1}$$

$$NEE = a_1 + a_2[T - \langle T \rangle] + C^* PRI^* \frac{a_3^* PAR}{a_4 + PAR}, \qquad B = a_5^* \exp\left(a_6^* \theta_{sfc}\right), \quad C = \frac{1 - \exp^{-a_6 \frac{\left(\theta_f - a_7\right)}{\left(1 - a_7\right)}}}{1 - \exp^{-a_6}}. \tag{D2}$$

[87] In equations (D1) and (D2), parameters a_1–a_4 and the drivers T, <T>, PAR, and PRI are defined as in the Model-0 equation (see above). The terms B and C define

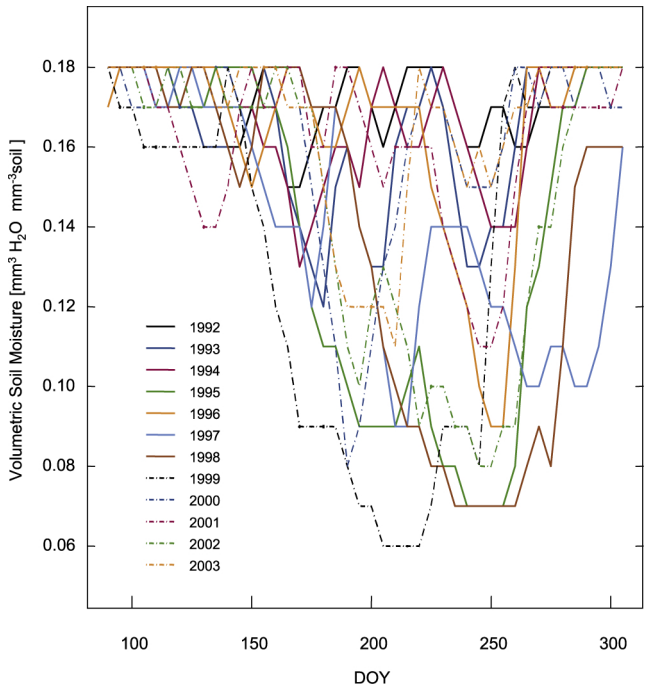

Figure D3. Calculated soil moisture in the lower layer of the soil moisture model for 1992–2003 at Harvard Forest. Note the dry anomalies in 1995, 1998, and 1999 with soil moisture dipping below 0.09. On the other hand, soil moisture in the summer of 1994 never dropped below 0.13.

response to soil moisture in Model-0a and Model-0b, respectively. Here θ_{sfc} is the soil moisture deficit of the surface layer in mm of H_2O, θ_f is the under layer soil moisture in terms of fractional field capacity (0–1), and a_5, a_6, a_7 are fitted parameters. Using nine years (1992–2000) of hourly, u* filtered NEE, T, PAR and reconstructed soil moisture observations, optimized parameters were derived for both Model-0b and Model-0a for the early, mid, and late summer seasons using a nonlinear least squares routine.

[88] The results for Model-0a and Model-0b were consistent. The optimized models improved model accuracy for NEE in midsummer by reducing modeled CO_2 uptake under dry soil conditions; however, the models failed to capture the afternoon depression in CO_2 uptake.

[89] To improve simulation of the physiological response of the ecosystem to soil moisture in the midsummer, a hydraulic resistor-based model of canopy water potential was coupled with a modified Model-0 equation (equations (D3) and (D4)). The data sets for NEE and driving variables (Ψ, PAR, T) were divided into 5-day aggregates, each of 24 hours (Appendix B). Water retention curves (K. E. Savage and E. A. Davidson, personal communication, 2000) were used to

Table D2. Midsummer Model-0 and Modified Model-0 With Moisture Stress Parameter (Model-0c) Optimized Parameters and Predicted NEE Versus Observed NEE Statistics for Hour and Season Timescale[a]

	Model-0/Model-0c Parameters								
	a1	a2	a3	a4	a5	A	B	Tmean	mean Ψ_C
Model-0	3.78	0.31	−40.0	879	NA	NA	NA	18.2	NA
Model-0c	4.35	0.03	−56.0	1033	0.05	0.02	0.08	18.2	−4.87
	Model-0/Model-0c Fit Statistics								
	N	<obs>	MAE	RMSE	b0	b0.se	b1	b1.se	R	rsq
					Hour Timescale					
Model-0	1944	−4.02	2.16	2.93	0.00	0.07	1.00	0.01	0.95	0.90
Model-0c	1944	−4.02	1.95	2.59	0.00	0.06	1.00	0.01	0.96	0.92
					Season Timescale					
Model-0	9	−4.02	0.48	0.56	−0.95	2.56	0.76	0.63	0.41	0.16
Model-0c	9	−4.02	0.24	0.34	0.71	1.14	1.18	0.28	0.84	0.70

[a]Goodness of fit is computed on the basis of 5-day aggregates, which is the time step for estimating soil moisture from transpiration and precipitation. N is number of valid observations used in calibration. Units are as follows: a1, $\mu moleCO_2\ m^{-2}\ s^{-1}$; a2, $\mu moleCO_2\ m^{-2}\ s^{-1}\ degC^{-1}$; a3, $\mu moleCO_2\ m^{-2}\ s^{-1}$; a4, μmole-photons $m^{-2}\ s^{-1}$; a5, MPa^{-1}; A, MPa m^2 s $umoleCO_2{}^{-1}\ hr^{-1}$; B, hr^{-1};mean T, °C; mean Ψ_C, MPa; <obs>, MAE, $\mu moleCO_2\ m^{-2}\ s^{-1}$. Here <obs> is mean of observations, RMSE is root mean square error, MAE is mean absolute error, and r is correlation coefficient; rsq = $\frac{var(res)}{var(obs)}$, where var(res) is variance of residuals and var(obs) is variance of observations; b0 and b1 (b0.se and b1.se) are intercept and slope (standard error) for linear regression of *Model-0/0c* predicted NEE versus observed NEE (NEE_{obs} = a0 + a1*NEE_{pred}).

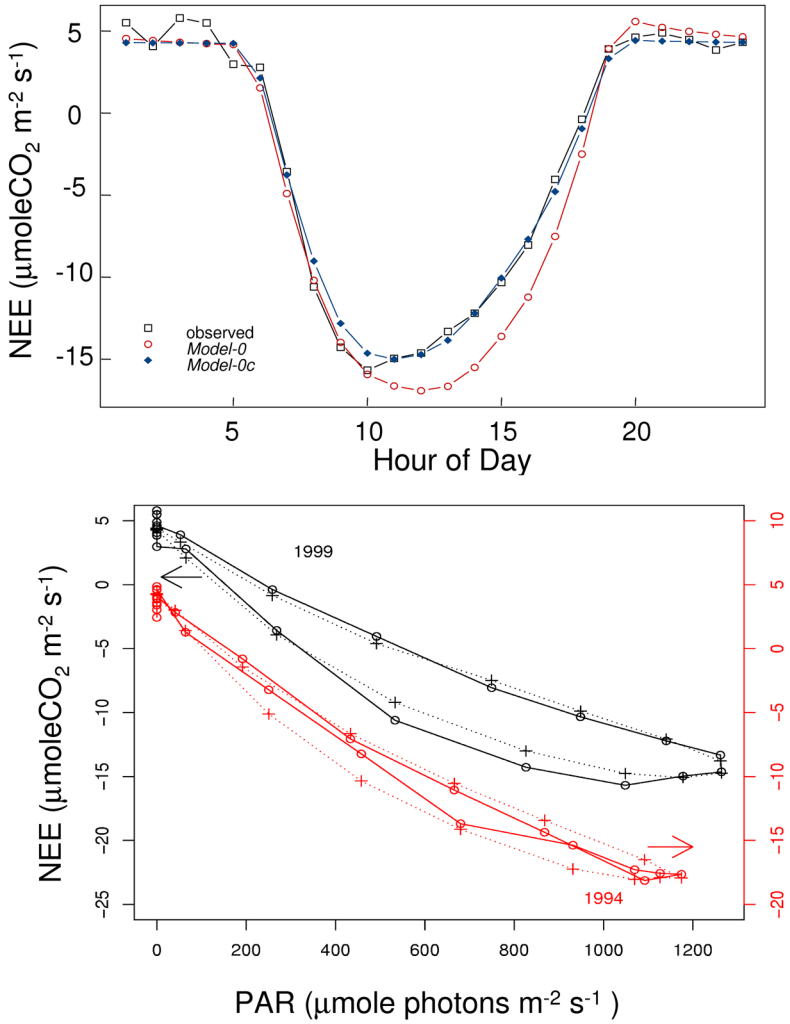

Figure D4. Predicted and observed daily pattern of NEE for mid summer. (top) Mean diurnal cycle observed and computed by Model-0 and Model-0c, in 1999, a dry year. (bottom) NEE versus incident light in a year with relatively dry soils (black, 1999) and wet soils (red, 1994, note offset by -5 μmole $m^{-2}s^{-1}$ for clarity), showing suppression of photosynthesis for given light level in the afternoon.

convert the hydrology model-estimated volumetric soil moisture to matric potential (Ψ_S). The daily canopy water potential was assumed to behave periodically and is estimated using equation (D3). The canopy matric potential (Ψ_C) was included as an additional term in the original Model-0 equation that modifies gross carbon assimilation (equation (D4)). Equations (D3) and (D4) were solved iteratively to obtain the optimized parameter set.

$$\frac{d\Psi_C}{dt} = (\Psi_S - \Psi_C)*B - A*E \tag{D3}$$

$$NEE = a_1 + a_2[T - \langle T\rangle] + \{1 + a_5*\Psi_C\}*\frac{a_3*PAR}{a_4 + PAR}. \tag{D4}$$

In equation (D3),

$$E = \{1 + a_5*\Psi_C\}*\frac{a_3*PAR}{a_4 + PAR}.$$

[90] In the hydraulic resistor equation, equations (D3) and (D4), Ψ_S and Ψ_C are the matric potential of the soil and canopy, the product EA is the canopy water transpiration rate, and B is the RC time constant for refilling the canopy with water. Model-0c uses GEE as a proxy for the canopy transpiration flux and parameter A is equivalent to $1/(\alpha C)$, where C is the canopy water capacitance and α is the canopy water use efficiency. The parameter a_5 controls the direction and magnitude of the Ψ_C influence on NEE.

[91] Model-0c improved model accuracy for NEE in midsummer by reducing modeled CO_2 uptake under dry soil conditions. The output of Model-0 with canopy matric potential is a significant improvement over the basic Model-0 on the season timescale, yielding a 45% reductions in RMSE and capturing *ca.* 70% of NEE interannual variability on the seasonal scale (Table D2). Model-0c even captured much of the diel cycle of NEE; under both dry (1999) and wet (1994) conditions, Model-0c captures the observed afternoon depression of NEE and the mean NEE diurnal cycle (Figure D4).

[92] **Acknowledgments.** This research was supported by the Office of Science (BER), U.S. Department of Energy, through the Northeast Regional Center of the National Institute for Global Environmental Change under Cooperative Agreement DE-FC02-03ER63613, and through the Terrestrial Carbon Program, DE-FG02-03ER83751, and by the National Science Foundation LTER program, grant DEB-0080592. C. J. K. was supported by a grant from the Office of Science, Biological and Environmental Research Program (BER), U.S. Department of Energy, through the South Central Regional Center of the National Institute for Global Environmental Change (NIGEC) under Cooperative Agreement DE-FC02-03ER63613. Financial support does not constitute an endorsement by DOE of the views expressed in this document. We thank the many participants involved in maintenance and operation of the HFEMS, and associated data collection, especially C. Jones, E. Gottlieb, B. Daube, A. Bright, D. Curran, and the Harvard Forest Woods Crew. Summer students engaged in collecting field data were supported by NSF Research Experience for Undergraduates (REU) program.

References

Adams, B., A. White, and T. M. Lenton (2004), An analysis of some diverse approaches to modeling terrestrial net primary productivity, *Ecol. Modell.*, *177*, 353–391.

Baker, T. R., et al. (2004), Increasing biomass in Amazonian forest plots, *Philos. Trans. R. Soc., Ser. B*, *359*, 353–365.

Ball, J. T. (1988), The ci/cs ratio: A basis for predicting stomatal control of photosynthesis, Ph.D. thesis, Stanford Univ., Stanford, Calif.

Barford, C. C., S. C. Wofsy, M. L. Goulden, J. W. Munger, E. Hammond-Pyle, S. P. Urbanski, L. Hutyra, S. R. Saleska, D. Fitzjarrald, and K. Moore (2001), Factors controlling long and short term sequestration of atmospheric CO_2 in a mid-latitude forest, *Science*, *294*, 1688–1691.

Bassow, S. L., and F. A. Bazzaz (1997), Intra- and inter-specific variation in canopy photosynthesis in a mixed deciduous forest, *Oecologia*, *109*, 507–515.

Battle, M., M. L. Bender, P. P. Tans, J. W. C. White, J. T. Ellis, T. Conway, and R. J. Francey (2000), Global carbon sinks and their variability inferred from atmospheric O_2 and delta ^{13}C, *Science*, *287*, 2467–2470.

Boone, R. D., K. Nadelhoffer, J. Canary, and J. Kaye (1998), Roots exert a strong influence on the temperature sensitivity of soil respiration, *Nature*, *396*, 570–572.

Bowden, R. D., K. Nadelhoffer, R. Boone, J. Melillo, and J. Garrison (1993), Contributions of aboveground litter, belowground litter, and root respiration to total soil respiration in a temperate mixed hardwood forest, *Can. J. For. Res.*, *23*, 1402–1407.

Braswell, B. H., D. S. Schimel, E. Linder, and B. Moore III (1997), The response of global terrestrial ecosystems to interannual temperature variability, *Science*, *278*, 870–872.

Brutsaert, W. H. (1975), On a derivable formula for long-wave radiation from clear skies, *Water Resour. Res.*, *11*, 742–744.

Cao, M., and F. I. Woodward (1998), Dynamic responses of terrestrial ecosystem carbon cycling to global climate change, *Nature*, *393*, 249.

Carroll, D. L. (1996), Chemical laser modeling with genetic algorithms, *AIAA J.*, *34*, 338–346.

Cavender-Bares, J., and F. A. Bazzaz (2000), Changes in drought response strategies with ontogeny in Quercus rubra: Implications for scaling from seedlings to mature trees, *Oecologia*, *124*, 8–18.

Ciais, P., P. P. Tans, M. Trolier, J. W. C. White, and R. J. Francey (1995), A large northern-hemisphere terrestrial CO_2 sink indicated by the C-13/C-12 ratio of atmospheric CO_2, *Science*, *269*, 1098–1102.

Collatz, G. J., J. T. Ball, C. Grivet, and J. A. Berry (1991), Physiological and environmental regulation of stomatal conductance, photosynthesis and transpiration: A model that includes a laminar boundary layer, *Agric. For. Meteorol.*, *53*, 107–136.

Collatz, G. J., M. Ribas-Carbo, and J. A. Berry (1992), Coupled photosynthesis-stomatal conductance model for leaves of C4 plants, *Aust. J. Plant Physiol.*, *19*, 519–538.

Davidson, E. A., and I. A. Janssens (2006), Temperature sensitivity of soil carbon decomposition and feedbacks to climate change, *Nature*, *440*, 165–173.

Davidson, E. A., I. A. Janssens, and Y. Luo (2006), On the variability of respiration in terrestrial ecosystems: Moving beyond Q_{10}, *Global Change Biol.*, *12*, 154–164, doi:10.1111/j.1365-2486.2005.01065.

Doney, S., K. Lindsay, I. Fung, and J. John (2006), A stable 1000 year coupled climate-carbon cycle simulation, *J. Clim.*, *19*, 3033–3054.

Dunn, A. L., C. C. Barford, S. C. Wofsy, M. L. Goulden, and B. C. Daube (2007), A long-term record of carbon exchange in a boreal black spruce forest: Means, responses to interannual variability, and decadal trends, *Global Change Biol*, doi:10.1111/j.1365-2486.2006.01221.x, in press.

Falge, E., et al. (2001a), Gap filling strategies for defensible annual sums of net ecosystem exchange, *Agric. For. Meteorol.*, *107*, 43–69.

Falge, E., et al. (2001b), Gap filling strategies for long term energy flux data sets, *Agric. For. Meteorol.*, *107*, 71–77.

Farquhar, G. D., S. von Caemmerer, and J. A. Berry (1980), A biochemical model of photosynthetic CO_2 assimilation in leaves of C_3 species, *Planta*, *149*, 78–90.

Field, C., and H. A. Mooney (1986), The photosynthesis-nitrogen relationship in wildplants, in *On the Economy of Plant Form and Function*, edited by T. J. Givnish, pp. 25–55, Cambridge Univ. Press, New York.

Foley, J. A., I. C. Prentice, N. Ramankutty, S. Levis, D. Pollard, S. Stitch, and A. Haxeltine (1996), An integrated biosphere model of land surface processes, terrestrial carbon balance, and vegetation dynamics, *Global Biogeochem. Cycles*, *10*, 603–628.

Freedman, J. M., D. R. Fitzjarrald, K. E. Moore, and R. K. Sakai (2001), Boundary layer clouds and vegetation-atmosphere feedbacks, *J. Clim.*, *14*, 180–197.

Friedlingstein, P., et al. (2006), Climate-carbon cycle feedback analysis: Results from the C4MIP model intercomparison, *J. Clim.*, *19*, 3337–3353.

Fung, I., S. C. Doney, K. Lindsay, and J. John (2005), Evolution of carbon sinks in a changing climate, *Proc. Natl. Acad. Sci. U. S. A.*, *102*, 11,201–11,206.

Giardina, C. P., and M. Ryan (2000), Evidence that decomposition rates of organic carbon in mineral soil do not vary with temperature, *Nature*, *404*, 858–861.

Goodale, C. L., et al. (2002), Forest carbon sinks in the Northern Hemisphere, *Ecol. Appl.*, *12*, 891–899.

Goulden, M. L., J. W. Munger, S.-M. Fan, B. C. Daube, and S. C. Wofsy (1996a), Effects of interannual climate variability on the carbon dioxide exchange of a temperate deciduous forest, *Science*, *271*, 1576–1578.

Goulden, M. L., J. W. Munger, S.-M. Fan, B. C. Daube, and S. C. Wofsy (1996b), Measurements of carbon storage by long-term eddy correlation: Methods and a critical evaluation of accuracy, *Global Change Biol.*, *2*, 169–182.

Gower, S. T. (2004), LAI field measurements for BigFoot MODIS Land Product Validations (Harvard Forest, Petersham, MA 2000-2002), http://mercury.ornl.gov/ornldaac/, Oak Ridge Natl. Lab. Distrib. Active Arch. Cent., Oak Ridge, Tenn.

Gower, S. T., R. E. McMurtrie, and D. Murty (1996), Aboveground net primary production decline with stand age: Potential causes, *Trends Ecol. Evol.*, *11*, 378–382.

Hicke, J. A., G. P. Asner, J. T. Randerson, C. Tucker, S. Los, R. Birdsey, J. C. Jenkins, C. Field, and E. Holland (2002), Satellite-derived increases in net primary productivity across North America, 1982-1998, *Geophys. Res. Lett.*, *29*(10), 1427, doi:10.1029/2001GL013578.

Hogberg, P., A. Nordgren, N. Buchman, A. F. S. Taylor, A. Ekblad, M. N. Hogberg, G. Nyberg, M. Ottosson-Lofvenius, and D. Read (2001), Large-scale forest girdling shows that current photosynthesis drives soil respiration, *Nature*, *411*, 789–792.

Houghton, R. A. (2000), Interannual variability in the global carbon cycle, *J. Geophys. Res.*, *105*, 20,121–20,130.

Houghton, R. A. (2002), Magnitude, distribution and causes of terrestrial carbon sinks and some implications for policy, *Clim. Policy*, *2*, 71–88.

Houghton, R. A., J. E. Hobbie, J. M. Melillo, B. Moore, B. J. Peterson, G. R. Shaver, and G. M. Woodwell (1983), Changes in the carbon content of terrestrial biota and soils between 1860 and 1980: A net release of CO_2 to the atmosphere, *Ecol. Monogr.*, *53*, 235–262.

Jackson, R. B., J. Canadell, and J. R. Ehleringer (1996), A global analysis of root distributions for terrestrial biomes, *Oecologia*, *108*, 389–411.

Jones, C. D., P. Cox, and C. Huntingford (2003), Uncertainty in climate-carbon-cycle projections associated with the sensitivity of soil respiration to temperature, *Tellus, Ser. B*, *55*, 642–648.

Jones, H. G. (1978), Modeling diurnal trends of leaf water potential in transpiring wheat, *J. Appl. Ecol.*, *15*, 613–626.

Joos, F., I. C. Prentice, S. Sitch, R. Meyer, G. Hooss, G.-K. Plattner, S. Gerber, and K. Hasselmann (2001), Global warming feedbacks on terrestrial carbon uptake under the Intergovernmental Panel on Climate Change (IPCC) emission scenarios, *Global Biogeochem. Cycles*, *15*, 891–907.

Keeling, C. D., J. F. S. Chin, and T. P. Whorf (1996), Increased activity of northern vegetation inferred from atmospheric CO_2 measurements, *Nature*, *382*, 146–149.

Kirschbaum, M. U. (1995), The temperature dependence of soil organic matter decomposition, and the effect of global warming on soil organic C storage, *Soil Biol. Biochem.*, *27*, 753–760.

Kirschbaum, M. U. (2004), Soil respiration under prolonged soil warming: Are rate reductions caused by acclimation or substrate loss?, *Global Change*, *10*, 1870–1877.

Knorr, W., I. C. Prentice, J. I. House, and E. A. Holland (2005), Long-term sensitivity of soil carbon turnover to warming, *Nature*, *433*, 298–301.

Krakauer, N. Y., and J. R. Randerson (2003), Do volcanic eruptions enhance or diminish net primary production? Evidence from tree rings, *Global Biogeochem. Cycles*, *17*(4), 1118, doi:10.1029/2003GB002076.

Kucharik, C. J., J. A. Foley, C. Delire, V. A. Fisher, M. T. Coe, S. T. Gower, J. Lenters, C. Molling, J. M. Norman, and N. Ramankutty (2000), Testing the performance of a dynamic global ecosystem model: Water balance, carbon balance, and vegetation structure, *Global Biogeochem. Cycles*, *14*, 795–825.

Kucharik, C. J., C. C. Barford, M. El Maayar, S. C. Wofsy, R. K. Monson, and D. D. Baldocchi (2006), Evaluation of a dynamic global vegetation model (dgvm) at the forest stand-level: Vegetation structure, phenology, and seasonal and inter-annual CO_2 and H_2O vapor exchange at three AmeriFlux study sites, *Ecol. Modell.*, *196*, 1–31.

Larcher, W. (1995), *Physiological Plant Ecology*, Springer, New York.

Law, B. E., et al. (2002), Environmental controls over carbon dioxide and water vapor exchange of terrestrial vegetation, *Agric. For. Meteorol.*, *113*, 97–120.

Lewis, S. L., et al. (2004), Concerted changes in tropical forest structure and dynamics: Evidence from 50 South American long-term plots, *Philos. Trans. R. Soc., Ser. B*, *359*, 421–436.

Liu, W. H., D. M. Bryant, L. R. Hutyra, S. R. Saleska, E. H. Pyle, D. Curran, and S. C. Wofsy (2006), Woody debris contribution to the carbon budget of selectively logged and maturing mid-latitude forests, *Oecologia*, *148*, 108–117.

Lloyd, J., and J. A. Taylor (1994), On the temperature-dependence of soil respiration, *Funct. Ecol.*, *8*, 315–323.

McGuire, A. D., III, I. C. Prentice, N. Ramankutty, T. Reichenau, A. Schloss, H. Tian, L. J. Williams, and U. Wittenberg (2001), Carbon balance of the terrestrial biosphere in the twentieth century: Analyses of CO_2, climate and land use effects with four process-based ecosystem models, *Global Biogeochem. Cycles*, *15*, 183–206.

Medvigy, D. (2006), The state of the regional carbon cycle: Results from a constrained coupled ecosystem-atmosphere model, Ph.D. thesis, Harvard Univ., Cambridge, Mass.

Miller, D. A., and R. A. White (1998), A conterminous United States multilayer soil characteristics dataset for regional climate and hydrology modeling, *Earth Interact.*, *2*(2), 1–26.

Moore, K. E., D. R. Fitzjarrald, R. K. Sakai, M. L. Goulden, J. W. Munger, and S. C. Wofsy (1996), Seasonal variation and turbulent exchange at a deciduous forest in Massachusetts, *J. Appl. Meteorol.*, *35*, 122–134.

Musselman, R. C., W. J. Massman, J. M. Frank, and J. L. Korfmacher (2005), The temporal dynamics of carbon dioxide under snow in a high elevation rocky mountain subalpine forest and meadow, *Arct. Antarct. Alp. Res.*, *37*, 527–538.

Myneni, R. B., J. Dong, C. J. Ticker, R. K. Kaufmann, P. E. Kauppi, J. Liski, L. Zhou, V. Alexeyev, and M. K. Hughes (2001), A large carbon sink in the woody biomass of Northern forests, *Proc. Natl. Acad. Sci. U. S. A.*, *98*, 14,784–14,789.

National Climate Data Center (2006), [http://lwf.ncdc.noaa.gov/oa/ncdc.html].

Palmer, W. C. (1965), Meteorological drought, *Res. Pap. 45*, 65 pp., U.S. Weather Bureau, Silver Spring, Md.

Parton, W. J., D. S. Schimel, and C. V. Cole (1987), Analysis of factors controlling soil organic matter levels in Great Plains grassland, *Soil Sci. Soc. Am. J.*, *51*, 1173–1179.

Pollard, D., and S. L. Thompson (1995), Use of a land-surface-transfer scheme (LSX) in a global climate model: The response to doubling stomatal resistance, *Global Planet. Change*, *10*, 129–161.

Prentice, I. C. (2001), et al The carbon cycle and atmospheric carbon dioxide, in *Climate Change 2001: The Scientific Basis. Contribution of Working Group I to the Third Assessment Report of the Intergovernmental Panel on Climate Change*, edited by J. T. Houghton et al., chap. 3, pp. 183–237, Cambridge Univ. Press, New York.

Reichstein, M., T. Katterer, O. Andren, P. Ciais, E. D. Schulze, W. Cramer, D. Papale, and R. Valentini (2005), Temperature sensitivity of decomposition in relation to soil organic matter pools: critique and outlook, *Biogeosciences*, *2*, 317–321.

Richardson, A. D., et al. (2006), A multi-site analysis of random error in tower-based measurements of carbon and energy fluxes, *Agric. For. Meteorol.*, *136*, 1–18.

Ruimy, A., P. G. Jarvis, D. D. Baldocchi, and B. Saugier (1996), CO_2 fluxes over plant canopies and solar radiation: A review, *Adv. Ecol. Res.*, *26*, 1–68.

Ryan, M. G. (1991), A simple method for estimating gross carbon budgets for vegetation in forest ecosystems, *Tree Physiol.*, *9*, 255–266.

Ryan, M. G., and B. E. Law (2005), Interpreting, measuring, and modeling soil respiration, *Biogeochemistry*, *73*, 3–27.

Ryan, M. G., D. Binkley, and J. H. Fownes (1997), Age-related decline in forest productivity: Pattern and process, *Adv. Ecol. Res.*, *27*, 213–262.

Sanderman, J., R. G. Amundson, and D. D. Baldocchi (2003), Application of eddy covariance measurements to the temperature dependence of soil organic matter mean residence time, *Global Biogeochem. Cycles*, *17*(2), 1061, doi:10.1029/2001GB001833.

Savage, K. E., and E. A. Davidson (2001), Interannual variation of soil respiration in two New England forests, *Global Biogeochem. Cycles*, *15*, 337–350.

Schimel, D., et al. (2000), Contribution of increasing CO_2 and climate to carbon storage by ecosystems in the United States, *Science*, *287*, 2004–2006.

Schimel, D. S., et al. (2001), Recent patterns and mechanisms of carbon exchange by terrestrial ecosystems, *Nature*, *414*, 169–172.

Sommerfeld, R. A., W. J. Massman, R. C. Musselman, and A. R. Mosier (1996), Diffusional flux of CO_2 through snow: Spatial and temporal variability among alpine-subalpine sites, *Global Biogeochem. Cycles*, *10*, 473–482.

Takagi, K., M. Nomura, D. Ashiya, H. Takahashi, K. Sasa, Y. Fujinuma, H. Shibata, Y. Akibayashi, and T. Koike (2005), Dynamic carbon dioxide exchange through snowpack by wind-driven mass transfer in a conifer-broadleaf mixed forest in northernmost Japan, *Global Biogeochem. Cycles*, *19*, GB2012, doi:10.1029/2004GB002272.

Tans, P. P., I. Y. Fung, and T. Takahashi (1990), Observational constraints on the global atmospheric CO_2 budget, *Science*, *247*, 1431–1438.

Tritton, L. M., and J. W. Hornbeck (1982), Biomass equations for major tree species of the northeast, *Gen. Tech. Rep. NE-69*, For. Serv., USDA, Washington, D. C.

Trumbore, S. (2006), Carbon respired by terrestrial ecosystems—Recent progress and challenges, *Global Change Biol.*, *12*, 141–153.

van Bochove, E., G. Theriault, P. Rochette, H. G. Jones, and J. W. Pomeroy (2001), Thick ice layers in snow and frozen soil affecting gas emissions from agricultural soils during winter, *J. Geophys. Res.*, *106*, 23,061–23,071.

Verberne, E. L. J., J. Hassink, P. De Willigen, J. J. R. Groot, and J. A. Van Veen (1990), Modeling organic matter dynamics in different soils, *Neth. J. Agric. Sci.*, *38*, 221–238.

Waring, R. H., and W. H. Schlesinger (1985), *Forest Ecosystems: Concepts and Management*, pp. 40–46, Elsevier, New York.

Whitehead, D., K. L. Griffin, M. H. Turnbull, D. T. Tissues, V. C. Engel, K. J. Brown, W. S. F. Schuster, and A. S. Walcroft (2004), Response of total night-time respiration to differences in total daily photosynthesis for leaves in a Quercus rubra L. canopy: Implications for modeling canopy CO_2 exchange, *Global Change Biol.*, *10*, 925–938.

Williams, M., E. B. Rastetter, D. N. Fernandes, M. L. Goulden, S. C. Wofsy, G. R. Shaver, J. M. Melillo, J. W. Munger, S.-M. Fan, and K. J. Nadelhoffer (1996), Modeling the soil-plant-atmosphere continuum in a Quercus-Acer stand at Harvard Forest: The regulation of stomatal conductance by light, nitrogen and soil/plant hydraulic properties, *Plant Cell Environ.*, *19*, 911–927.

Wofsy, S. C., and R. C. Harriss (2002), The North American Carbon Program (NACP): A report of the NACP committee of the U.S. Carbon Cycle Science Steering Group, report, 62 pp., U. S Global Change Res. Program, Washington, D. C.

Wofsy, S. C., M. L. Goulden, J. W. Munger, S. M. Fan, P. S. Bakwin, B. C. Daube, S. L. Bassow, and F. A. Bazzaz (1993), Net exchange of CO_2 in a midlatitude forest, *Science*, *260*, 1314–1317.

Xiao, X., Q. Zhang, B. Braswell, S. Urbanski, S. Boles, S. Wofsy, and D. Ojima (2004), Modeling gross primary production of temperate deciduous broadleaf forest using satellite images and climate data, *Remote Sens. Environ.*, *91*, 256–270.

C. Barford and C. Kucharik, Center for Sustainability and the Global Environment (SAGE), Nelson Institute for Environmental Studies, 1710 University Avenue, University of Wisconsin-Madison, Madison, WI 53726, USA.

J. Budney, K. McKain, J. W. Munger, E. Pyle, and S. Wofsy, Division of Engineering and Applied Sciences and Department of Earth and Planetary Sciences, Harvard University, Cambridge, MA 02138, USA.

M. Czikowsky and D. Fitzjarrald, Atmospheric Sciences Research Center, State University of New York at Albany, Albany, NY 12203, USA.

S. Urbanski, Fire Sciences Laboratory, USDA Forest Service, 5775 W U. S. Highway 10, Missoula, MT 59808, USA. (surbanski@fs.fed.us)